学位論文

Structure and stability of aluminum clusters containing icosahedral units

(正二十面体ユニットを含む アルミニウムクラスターの構造と安定性)

平成26年12月博士（理学）申請

東京大学大学院理学系研究科
化学専攻

渡辺 智美

Abstract

Clusters of simple metals such as Na, Au, and Al gain high stability when the superatomic orbitals are completely filled with the valence electrons. Al_{13}^-, one of the most extensively studied magic clusters, has a closed electronic configuration with 40 valence electrons and a highly symmetrical icosahedral motif. In addition, Al_{13}^- is known to be robust against oxidation by O_2, whereas other Al_n^- are easily etched into smaller clusters by consecutively release of Al_2O fragments. Thus, Al_{13}^- has attracted much attention as a building unit of cluster-based nanomaterials. Although several Al_{13}-containing complexes such as $Al_{13}Na$ and $Al_{13}I^-$ have been successfully formed in gas phase, chemical synthesis of Al_{13}-based materials has been a challenge in cluster science. The aim of the thesis is to provide a clue for the synthesis of Al_{13}-based materials by a combined approach of experimental results and theoretical calculations.

In chapter 2, I studied reactions of Al_n^- under high-pressure O_2 to gain insights into the stability of Al_n^- under atmospheric conditions. Aluminum cluster anions were generated by laser vaporization and were allowed to pass through a cell in which O_2 was filled. Compositions of the reaction products were determined by time-of-flight mass spectrometer. The reaction of Al_n^- and O_2 under a high-pressure condition yielded the previously unknown aluminum oxides $Al_{14}O^-$ and $Al_{15}O_2^-$. Photoelectron spectroscopy and density functional theory calculations revealed that $Al_{14}O^-$ and $Al_{15}O_2^-$ are composed of an icosahedral Al_{13} moiety bonded by one and two OAl unit(s), respectively. The preferential formation of $Al_{14}O^-$ and $Al_{15}O_2^-$ was due to their high stability associated with the Al_{13} moiety and the efficient dissipation of reaction exothermicity by collisional cooling.

In chapter 3, I computationally investigated the interaction between Al_{13} and electron donating ligand to stabilize open-shell Al_{13} by electronic shell closure. From the density functional theory calculations of structures of Al_{13} coordinated by ligand with carbonyl group, it was found that ligands with nitrogen atom or two carbon atoms next to carbonyl group can donate electron to Al_{13}. Then the structures of $Al_{13}(EP)_n$ (n = 0–4), which EP (*N*-ethyl-2-pyrrolidone) is a model of polymer, were extensively investigated. The optimized structure of $Al_{13}(EP)_1$ indicated that the EP ligand is chemisorbed to the atop site of Al_{13} via the carbonyl O atom, while donating –0.36 e to the Al_{13} moiety. The chemisorption to the Al_{13} moiety is energetically preferred up to three EP ligands and the total charge accumulated in Al_{13} reaches nearly –1 e in $Al_{13}(EP)_3$. The fourth EP ligand, however, prefers to be bound to one of the chemisorbed EP ligands via electrostatic interaction rather than to be chemisorbed on Al_{13}. The switchover of the bonding scheme of EP at $Al_{13}(EP)_4$ suggests that this phenomenon is associated with closure of electronic shell of the Al_{13} moiety in $Al_{13}(EP)_3$. However, spin density analysis revealed that the superatomic orbital 1F of Al_{13} remains singly occupied even after chemisorption of three EP ligands. In conclusion, chemisorption of EP ligands to Al_{13} does not lead to the filling of the superatomic orbital 1F, but formally donates electronic charge through polarized Al–O bonding.

In chapter 4, I described concluding remarks of the present works.

Contents

Chapter 1.

General introduction

1.1 Potential of nanoparticles and clusters

The field of nanotechnology is one of the most active research areas. Nanoparticles, whose diameters are in the range of 1–100 nm, are located at between an atom and bulk material (Figure 1.1). Metal nanoparticles are applicable to new materials such as catalysts,[1–3] optical devices,[4,5] magnetic materials,[6,7] and bioimaging systems[8,9] because they show attractive properties different from corresponding bulk metal. The discovery in 1987 by Haruta and co-workers that small gold particles with 5 nm supported on metal oxide could catalyze CO oxidation even at –70 °C[10] encouraged many researchers to reduce the size of metal particles as small as possible.

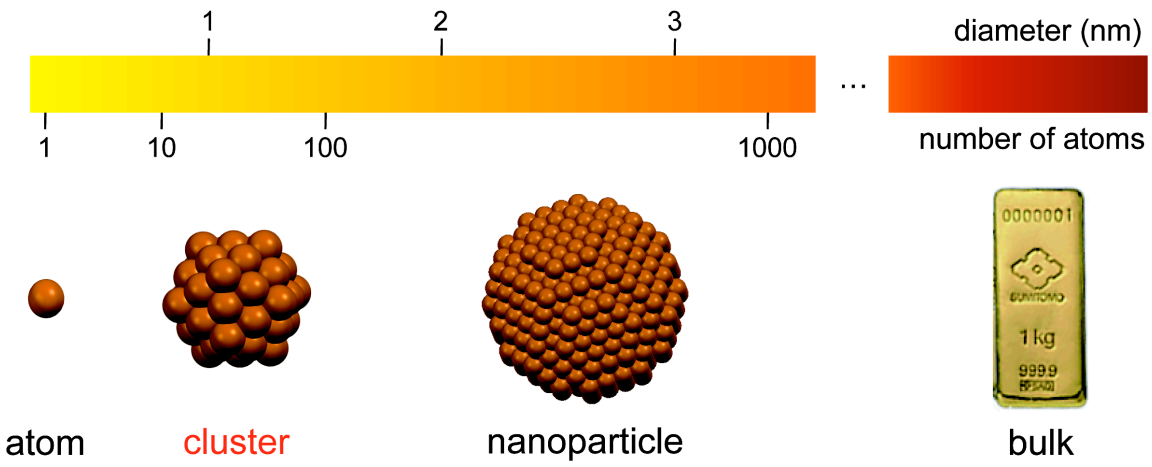

Figure 1.1. Relationship between atom, cluster, nanoparticle, and bulk.

The particle smaller than about 2 nm and composed of several to few hundred of atoms is called “cluster”. Clusters are classified into several categories such as metal cluster, covalent cluster, ionic cluster, van der Waals cluster, molecular cluster, organometallic cluster, and so on, depending on the nature of interaction between the constituent units. It is known that clusters exhibit novel properties different from not

only atom and bulk but also nanoparticles because of their unique geometrical structure and discrete electronic structure. The discovery in gas phase experiment and the subsequent large-scale synthesis of C_{60} fullerene[11–13] have led to initiated active research on nanocarbon materials including nanotube and graphene. These nanocarbon materials show quite different properties from bulk materials (diamond and graphite) and will find application in wide areas of technology and science.

Spherical clusters are regarded as a "superatom". A concept of superatom was firstly introduced as artificial atoms of semiconductor heterostructure by Watanabe and Inoshita.[14] They defined superatom as a quasi-atomic system that electrons transferred from donor doped in spherical core to surrounding matrix with larger electron affinity are accommodated in quantized orbital of potential produced by the ionized core. Khanna and Jena were pioneers of applying this concept to clusters.[15] They suggested that superatoms can form building block of three-dimensional periodic table as superhalogens, superalkalis, and, superatomic alkaline-earth metals instead of halogens, alkali metals, and alkaline-earth metals of Mendeleev's periodic table, respectively.[16–18]

1.2 Free metal clusters

1.2.1 Generation of free metal clusters

Cluster science has greatly developed in a few decades. The clusters isolated in vacuum are often used for investigating intrinsic features because of no interaction with surroundings. The knowledge about bare clusters is important in understanding properties in condensed phase. Generation of metal clusters in gas phase is conducted by various methods such as seeded supersonic expansion method, gas-aggregation method, laser vaporization method, and electrical arc discharge method.[19] The basic

principle of metal cluster generation is that metal atoms vaporized from bulk are aggregated and cooled by supersonic jet. Any size of clusters can be generated in principle depending on conditions. The metal clusters thus generated can be analyzed by coupling with apparatus such as mass spectrometer, infrared spectrometer, photoelectron spectrometer, photodissociation spectrometer, and surface-induced dissociation instrument.

1.2.2 Stability of free metal clusters

In the last few decades, both experimental and theoretical studies have been conducted extensively about stability, reactivity, and properties of metal clusters. One of the earliest works was reported by Knight and co-workers in 1984.[20] They measured mass spectra of sodium clusters (Na_n, n is the number of atoms in the cluster) produced in gas phase and found that the clusters showed high mass abundance at specific numbers of n, 8, 18, 20, 34, 40, … as shown in Figure 1.2. The clusters that are more stable than surrounding size are called magic clusters. The magic numbers of Na_n were explained successfully by electronic shell closure of the clusters orbital. The valence electrons of clusters behave as nearly free electrons in jellium-like potential made by uniform positive charged sphere and occupy the quantized orbitals.[19,21–23] According to this concept, the electronic shells are closed when the number of electrons is 2, 8, 18, 20, 34, 40, 58, 68, 70, … because corresponding superatomic orbitals, 1S, 1P, 1D, 2S, 1F, 2P, 1G, 2D, 3S … are completely filled, respectively, and the electronic shell closure makes the cluster stable. In case of Na_n, because Na is monovalent element ($[Ne](3s)^1$) the stability of clusters is expected to be enhanced with n = 2, 8, 18, 20, … same with the number of valence electrons as shown in the previous experiments. This electron

counting rule can be applied to other simple metals such as Au,[24,25] Mg,[26] and Al.[26,27] For example, Au is also monovalent element ($[Xe](4f)^{14}(5d)^{10}(6s)^{1}$) and the magic number of Au clusters is known to be 8, 18, 20, … and so on.

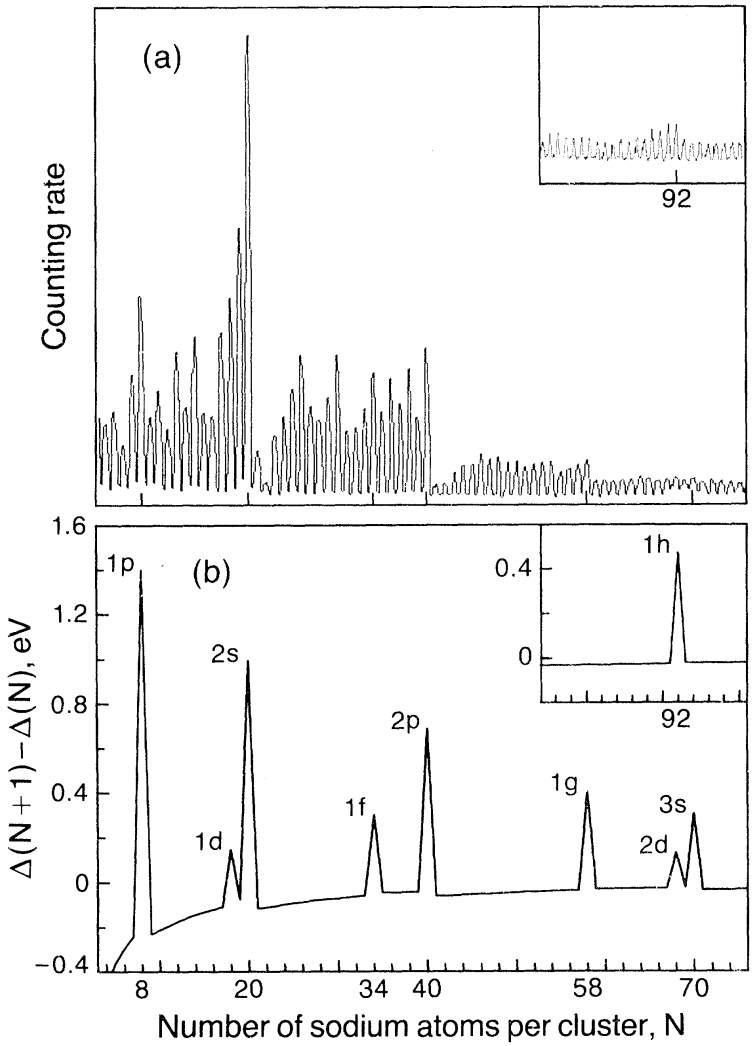

Figure 1.2. (a) Positive ion mass spectrum of sodium clusters and (b) the calculated change in the electronic energy difference.[20]

On the other hand, the magic number of Na_n larger than n = 3000 is different from those expected from electronic shell closure (Figure 1.3).[28] In this size regime, the

atomic packing determines the stability of the clusters. The clusters are stable when they take complete icosahedral motif. In summary, the stability of small ($n \leq 1500$) clusters is determined by the closure of electronic shells, whereas that of larger clusters is governed by closure of geometrical shells.

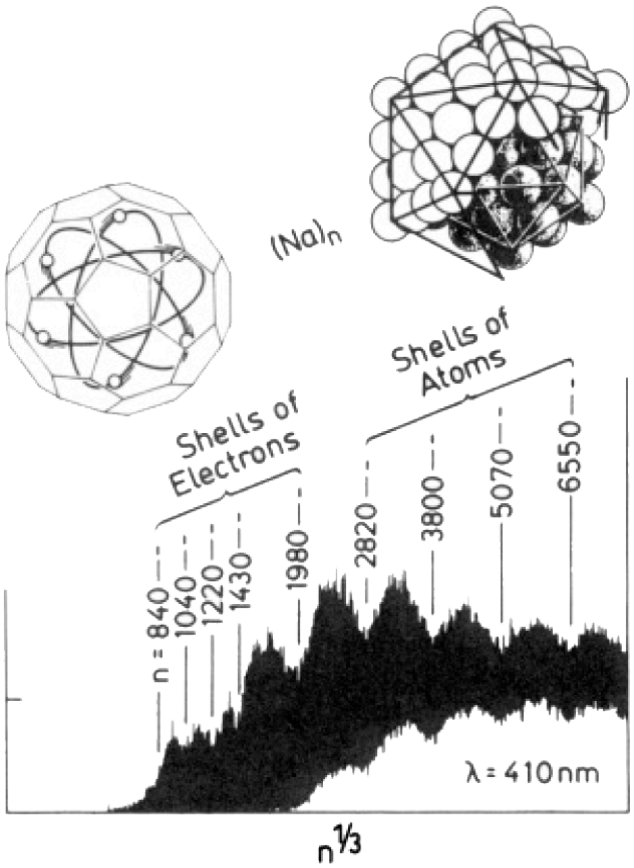

Figure 1.3. Mass spectra of photoionized Na_n. Two sequences of structures are observed at equally spaced intervals on the $n^{1/3}$ scale – an electronic shell sequence and a structural shell sequence.[28]

1.2.3 Reactivity of free metal clusters

In gas phase experiments, the number of atoms can be controlled and determined at atomic level. The difference of the number of atoms, even one atom,

arises the drastic difference of not only stability but also reactivity of the clusters. The chemical reactivity of metal clusters with oxygen (O_2) has gained interests since it is important for understanding the stability in air and catalytic activity for oxidation reactions. Figures 1.4(a) and 1.4(b) show the reactivity of Au_n^- against O_2 and the electron affinities of Au_n^-, respectively.[29] Au_n^- with only the even number of anions except for n = 16 reacted with O_2 and the reactivity was correlated obviously to the electron affinities of Au_n^-.[30,31] The results of photoelectron spectroscopy of adduct species $Au_nO_2^-$ revealed that the unpaired electron of even numbered Au cluster anion was partially donated to O_2.[32]

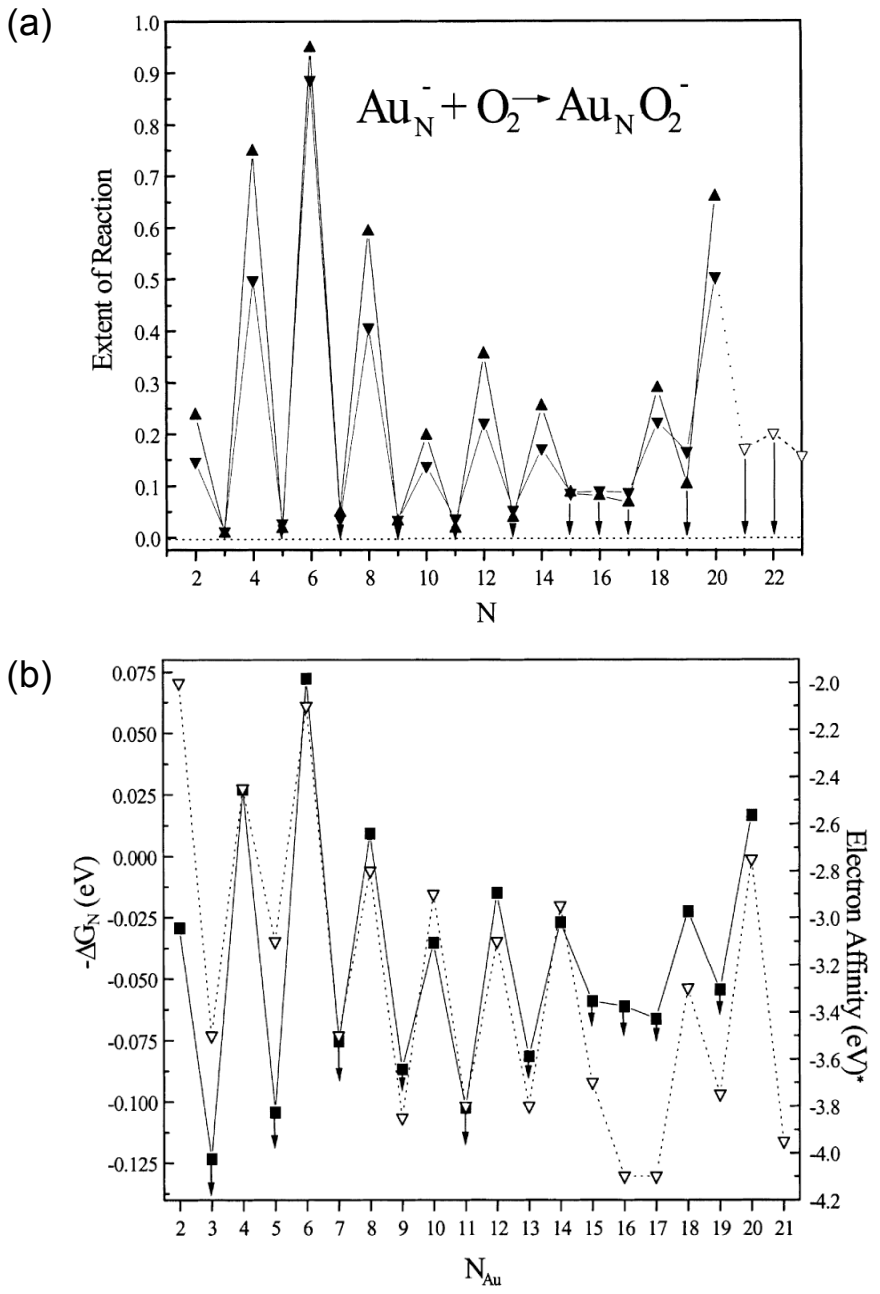

Figure 1.4. (a) Cluster-size dependence of the reaction of Au cluster anions with O_2. The separate plots correspond to different O_2 concentration. (b) Cluster-size dependence of the free energy of the reaction of Au cluster anions with O_2 (—, left axis) and the measured electron affinities of Au cluster anions (⋯, right axis).[29]

1.3 Protected metal clusters

1.3.1 Synthesis of protected metal clusters

To apply metal clusters as functional materials, it is necessary to obtain them in condensed phase. There are several methods for preparing metal nanoparticles and clusters in condensed phase such as reduction method,[33] laser ablation method,[34,35] hydrothermal synthesis method,[36] and gas condensation method.[37,38] Among them, the reduction method that reduces metal precursor ions by reducing agent is often used to synthesize metal clusters because the size distribution or chemical composition can be controlled depending on conditions. Although some of metal clusters are predicted to be more stable than neighbors, bare metal clusters are unstable against aggregation in order to reduce surface energy. The crucial issue for the synthesis and practical application of metal clusters is to stabilize the clusters against aggregation or sintering. A typical method of stabilization is protection by organic ligands or immobilization on solid supports. Recently, the synthesis of Au and Ag clusters protected by ligand such as thiolate (SR), halogen, and phosphine (PR_3) has advanced dramatically.[39–42] The synthesized clusters are characterized by mass spectrometry with electrospray ionization and matrix-assisted laser desorption ionization, powder X-ray diffraction analysis, transmission electron microscopy, ultraviolet-visible spectroscopy, and so on. So far, a lot of protected metal clusters were precisely synthesized and determined the atomic structures, for instance $[Au_{11}(PR_3)_8Cl_2]^+$,[43] $[Au_{13}(PR_3)_{10}Cl_2]^{3+}$,[44] $[Au_{25}(SR)_{18}]^-$,[45,46] $Au_{38}(SR)_{24}$,[47] $Au_{102}(SR)_{44}$,[48] and $[Ag_{44}(SR)_{30}]^{4-}$.[41,42]

1.3.2 Stability of protected metal clusters

The ligands not only sterically protect the clusters from aggregation but also

electronically stabilize the clusters by adjusting the formal number of the valence electrons confined in the clusters. The stability of the ligand-protected metal clusters can be explained by a simple scheme proposed by Häkkinen and co-workers based on the superatomic concept.[49] They defined the total numbers of valence electrons (n^*) of $[A_NX_ML_S]^Z$ by the following equation:

$$n^* = N \times V_A - M - Z \qquad (1.1)$$

where N, M, and S are the numbers of atoms of metal A, ligands X that withdraw electrons from metal core, and ligands L that coordinate to the metal core without withdrawing electrons, respectively, Z is a net charge and V_A is the number of valence electrons in a single metal atom. Given that each thiolate or halogen ligand takes one electron from the metal core, the n^* values in ligand-protected Au and Ag clusters agree, in most cases, with those predicted from the spherical electronic shell model. For example, the core of $[Au_{25}(SR)_{18}]^-$ is determined by single-crystal X-ray diffraction analysis to be icosahedral Au_{13} and its n^* value is calculated to be 8 with $1S^21P^6$ (Figure 1.5).[45,46,50]

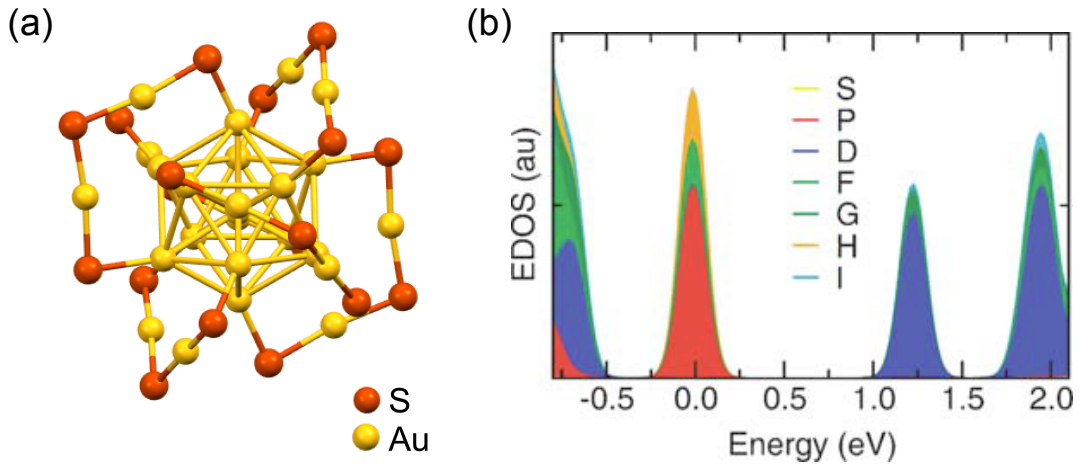

Figure 1.5. (a) Single-crystal structure[45] and (b) electron density of states of $[Au_{25}(SR)_{18}]^{-}$.[50]

1.4 The present study

1.4.1 Why aluminum?

Aluminum is expected to replace to precious metal because it is a ubiquitous element and cheap metal. Al nanoparticles that are stable under ambient conditions have gained interests as energetic materials,[51–56] optical devices,[57–59] and hydrogen storage/generating materials.[60,61] However, Al reacts readily with oxygen while releasing a huge amount of heat and produces aluminum oxide on the surface with following equation.

$$4Al + 3O_2 \rightarrow 2Al_2O_3,\ \Delta H = -1675.7\ \text{kJ/mol} \qquad (1.2)$$

To prevent oxidation of the surface, Al nanoparticles are passivated by organic reagents, such as poly(vinylpyrrolidone) (PVP),[55] poly(methylmethacrylate),[55] oleic acid,[61] and isophthalic acid[62] or by embedded in matrices of ammonium nitrate and ammonium perchlorate.[56]

1.4.2 Stability of free aluminum clusters

The electron configuration of Al atom is $[Ne](3s)^2(3p)^1$. It was found from the study of photoelectron spectroscopy of Al clusters that each Al atoms in Al_n ($n \geq 9$) provide three valence electrons because of the hybridization of 3s and 3p orbitals.[63] In contrast, the theoretical study indicated that the transition of behavior from monovalent to trivalent occurred with n between 5 and 7.[64] Then, the numbers of valence electrons in magic clusters such as Al_7^+, Al_{13}^-, and Al_{23}^- are calculated to be 20, 40, and 70 electrons, respectively. In particular, Al_{13}^-, which is regarded as superatomic noble gas, is quite stable because of not only the electronic shell closure with 40 electrons but also the icosahedral structure (Figure 1.6).

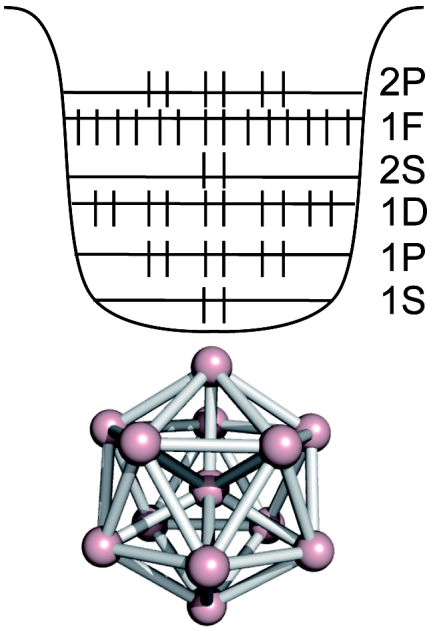

Figure 1.6. Schematic description of the electronic and geometrical structure of Al_{13}^-.

1.4.3 Reactivity of free aluminum clusters

Atomic level understanding has been obtained for the reaction of Al clusters

with O_2 under single collision condition through the pioneering works of Castleman and co-workers.[65,66] Al cluster cations and anions were etched into smaller clusters during the oxidation, corresponding to the combustion of Al powders. Figure 1.7 shows the etching reaction of Al cluster anions with O_2 and the following reaction paths were well established.[67,68]

$$Al_n^- + O_2 \rightarrow Al_{n-1}O + AlO^- \text{ or } Al_{n-1} + AlO_2^- \ (n \leq 7) \quad (1.3)$$

$$Al_n^- + O_2 \rightarrow Al_{n-4}^- + 2Al_2O \quad (n \geq 8) \quad (1.4)$$

Interestingly, magic clusters such as Al_7^+, Al_{13}^-, and Al_{23}^- showed high tolerance for O_2 in contrast to the efficient oxidation of Al nanoparticles. Such inertness toward O_2 has been attributed to the closure of electronic shells for the clusters. On the other hand, Schnöckel and co-workers reported that Al_{13}^- was degraded to Al_9^- with releasing $2Al_2O$ in the presence of excited O_2.[69] Theoretical studies have shown that the chemical inertness of aluminum magic clusters is due to the barrier required for transition of the spin states from triplet intermediates to singlet products in $^1Al_{13}^- + {}^3O_2 \rightarrow {}^3[Al_{13}{\cdot}O_2]^- \rightarrow {}^1Al_9^- + 2Al_2O$ as shown in Figure 1.8.[69–73]

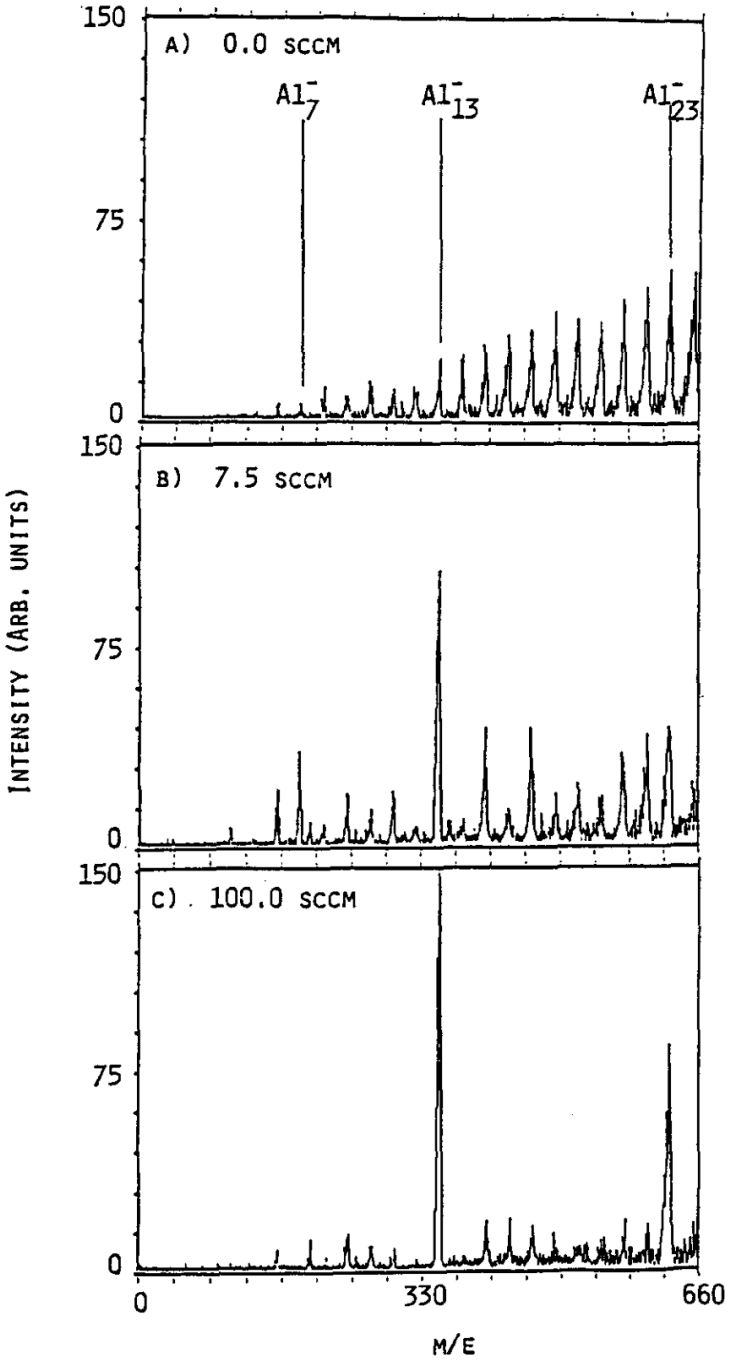

Figure 1.7. Series of mass spectra showing progression of etching reaction of Al_n^- with O_2.[65]

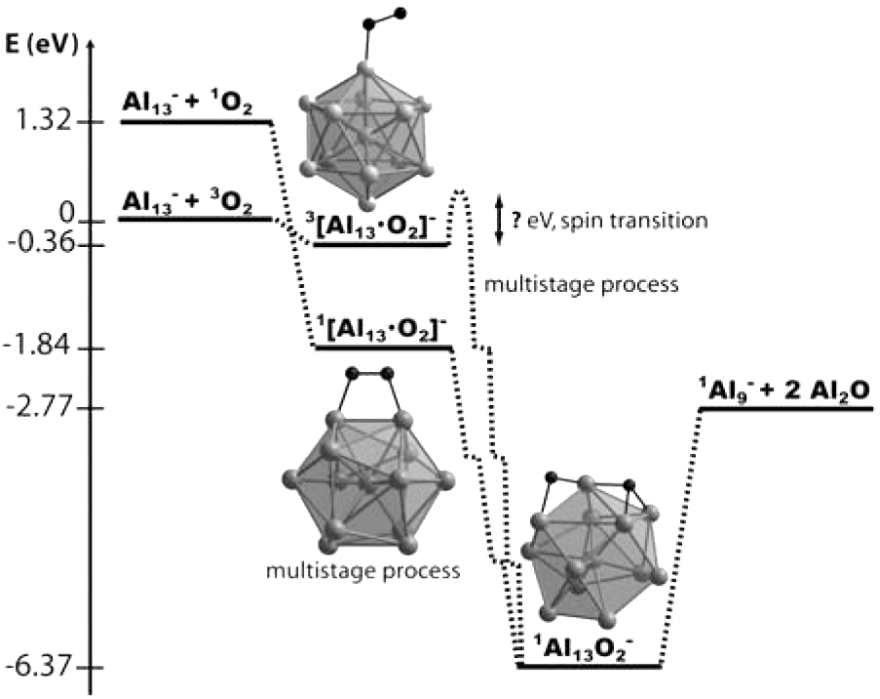

Figure 1.8. Energy diagram (calculated) for the interaction of $^1O_2$ and $^3O_2$ on the Al_{13}^- cluster surface.[69]

In contrast to the reaction of Al_n^- with O_2, the reactivity of Al_n^- with water was found to depend on geometrical structure rather than electronic shell structure.[74,75] The size-dependent reactivity of Al clusters for absorption of one or more water can be attributed to the dissociative chemisorption of water at specific surface sites. On the other hand, icosahedral Al_{13}^- still showed high resistance to water with large barriers because of no complementary active sites. In addition, Al_{13}^- is unreactive even in the reaction with other molecules such as methanol,[76,77] hydrogen iodide,[78] and ammonia,[79] while other sized Al_n^- are easier to form adduct species and as a result dissociative species.

1.4.4 Synthesis of protected aluminum clusters

Schnöckel and co-workers synthesized small Al clusters protected by ligands called metalloid clusters, $Al_4Cp^*_4$, $Al_8Cp^*_4$, $SiAl_{14}Cp^*_6$, and $Al_{50}Cp^*_{12}$ (Figure 1.9) (Cp* = pentamethylcyclopentadienyl).[80–83] The *n** values of these clusters are calculated to be 8, 20, 40, and 138, respectively, by assuming that each Al atom and Si atom provides three and four valence electrons, respectively, while each Cp* ligand takes one electron from the Al clusters.[84] These *n** values are same with those predicted from electronic shell closure so that these clusters are expected to show high stability even in an atmosphere. However, the above metalloid clusters are easily oxidized in air although these are theoretically demonstrated that by employing Cp* the oxidation rates are retarded as compared with the less-bulky cyclopentadienyl ligand.[85]

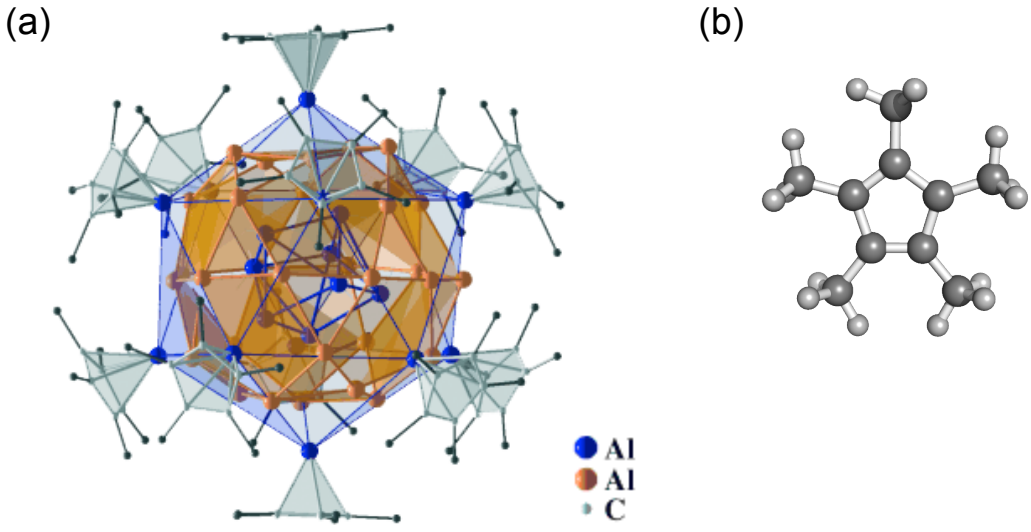

Figure 1.9. (a) Single-crystal structure of $Al_{50}Cp^*_{12}$ and (b) structure of Cp* (pentamethylcyclopentadienyl).[82]

1.4.5 Why Al_{13} superatom?

Magic cluster Al_{13}^- is a potential candidate of building block for air-stable Al clusters because of both intrinsic stability and chemical stability under single collision condition as shown in sections 1.4.2 and 1.4.3. Now the challenge to producing Al_{13}^- is how we can externally supply one extra electron to open-shell Al_{13}. The simplest way of supplying one electron to Al_{13} is to dope an alkali metal atom. Actually, the formation of $Al_{13}X$ (X = H, Au, and alkali metals)[86,87] in the gas phase has been reported by Nakajima and Bowen (Figure 1.10). In addition, Al_{13}^+ moiety of $Al_{13}H_2O^+$, which is a product of the reaction between Al_n^+ and water, was also stabilized by lone-pair electrons of water.[88] Here I consider to stabilize Al_{13} by an electron-donating ligand, such as PVP: it has been demonstrated experimentally that Pt clusters[89,90] and Au clusters[91,92] stabilized by PVP are negatively charged (Figure 1.11), and it has been predicted theoretically that Au_{13} is negatively charged by electron transfer from PVP.[93]

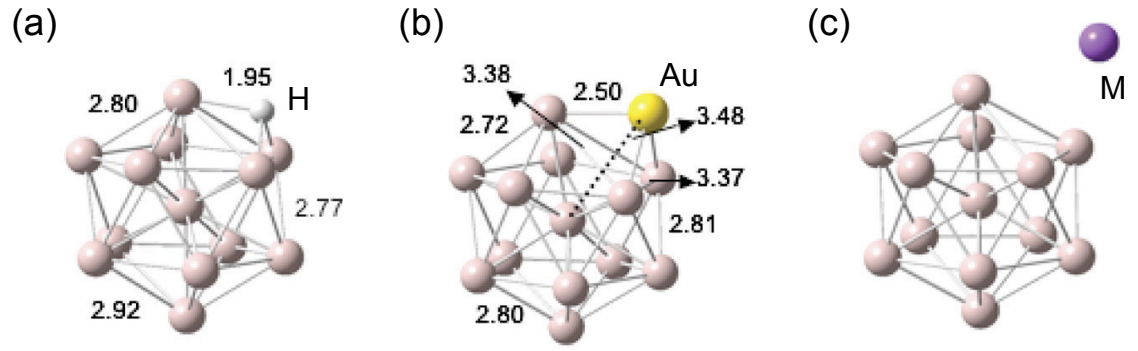

Figure 1.10. Optimized Structures of $Al_{13}X$. X = (a) H, (b) Au, and (c) M (M = Li, Na, K, Rb, and Cs).[87]

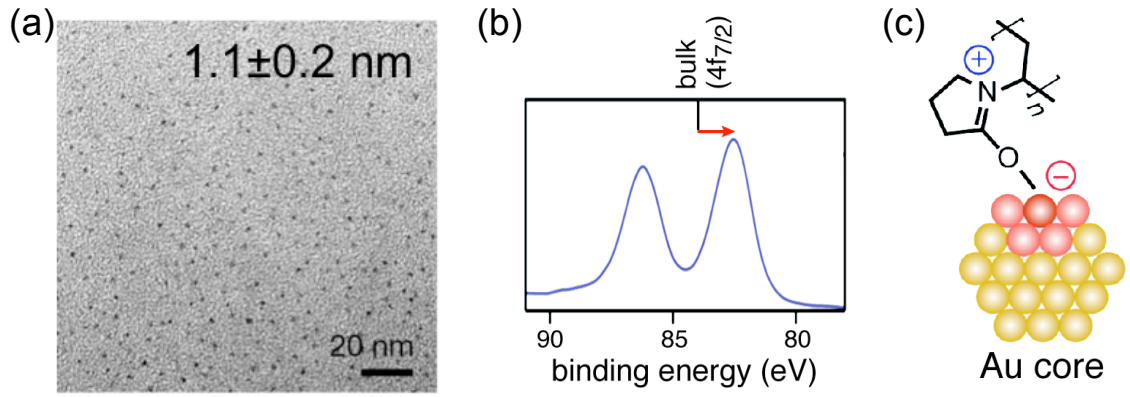

Figure 1.11. (a) TEM image, (b) XPS spectrum of Au cluster stabilized by PVP, and (c) schematic of electron transfer to Au cluster from PVP.[92]

1.4.6 Aim of the present study

The synthesis of ligand-protected aluminum clusters under inert gas has been reported as described in section 1.4.4. However, there are still difficulties on the synthesis of aluminum clusters so the examples of the synthesis are very limited. Moreover the synthesized aluminum clusters are unstable in air. In order to obtain stable aluminum cluster based materials, we have to develop methods to size control synthesis and stabilization against oxidation.

The aim of the present work is to obtain a hint toward synthesis of superatomic Al_{13}-based materials (Figure 1.12). In chapter 2, chemical reactions of Al_n^- under high-pressure O_2 were investigated to gain insights into the stability of Al_{13}^- under atmospheric conditions. In chapter 3, interaction between open-shell Al_{13} and electron donating ligand with carbonyl group was studied by density functional theory (DFT) calculations to test the hypothesis that the electronic shell of Al_{13} can be closed by electron donation from ligands.

Obtaining clues toward synthesis of Al_{13}-based materials

Chapter 2. Stability of Al_{13}^- under high-pressure O_2

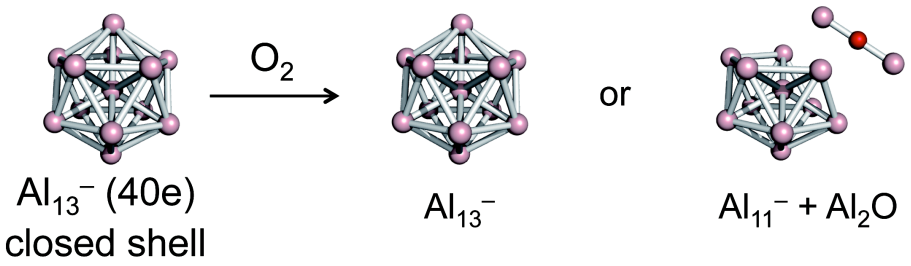

Chapter 3. Stabilization of Al_{13} by electron donating ligand

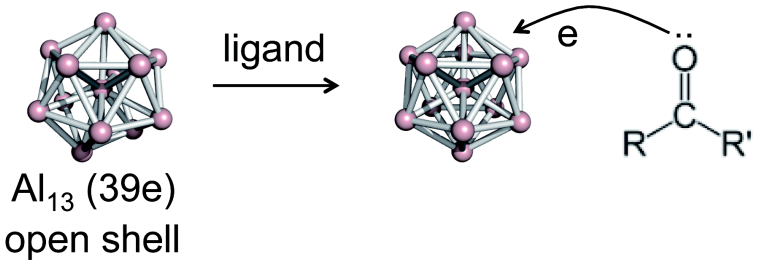

Figure 1.12. Aim of the present work.

References

1. Joo, S. H.; Park, J. Y.; Renzas, J. R.; Butcher, D. R.; Huang, W.; Somorjai, G. A. *Nano Lett.* **2010**, *10*, 2709.
2. Kesavan, L.; Tiruvalam, R.; Ab Rahim, M. H.; bin Saiman, M. I.; Enache, D. I.; Jenkins, R. L.; Dimitratos, N.; Lopez-Sanchez, J. A.; Taylor, S. H.; Knight, D. W.; Kiely, C. J.; Hutchings, G. J. *Science* **2011**, *331*, 195.
3. Mitsudome, T.; Takahashi, Y.; Ichikawa, S.; Mizugaki, T.; Jitsukawa, K.; Kaneda, K. *Angew. Chem., Int. Ed.* **2013**, *52*, 1481.
4. Rycenga, M.; Cobley, C. M.; Zeng, J.; Li, W.; Moran, C. H.; Zhang, Q.; Qin, D.; Xia, Y. *Chem. Rev.* **2011**, *111*, 3669.
5. Chen, H. M.; Chen, C. K.; Chen, C. J.; Cheng, L. C.; Wu, P. C.; Cheng, B. H.; Ho, Y. Z.; Tseng, M. L.; Hsu, Y. Y.; Chan, T. S.; Lee, J. F.; Liu, R. S.; Tsai, D. P. *ACS Nano* **2012**, *6*, 7362.
6. Sun, S.; Murray, C. B.; Weller, D.; Folks, L.; Moser, A. *Science* **2000**, *287*, 1989.
7. Lu, A. H.; Salabas, E. L.; Schüth, F. *Angew. Chem., Int. Ed.* **2007**, *46*, 1222.
8. Cao, L.; Wang, X.; Meziani, M. J.; Lu, F.; Wang, H.; Luo, P. G.; Lin, Y.; Harruff, B. A.; Veca, L. M.; Murray, D.; Xie, S. Y.; Sun, Y. P. *J. Am. Chem. Soc.* **2007**, *129*, 11318.
9. Zrazhevskiy, P.; Sena, M.; Gao, X. *Chem. Soc. Rev.* **2010**, *39*, 4326.
10. Haruta, M.; Kobayashi, T.; Sano, H.; Yamada, N. *Chem. Lett.* **1987**, 405.
11. Kroto, H. W.; Heath, J. R.; O'Brien, S. C.; Curl, R. F.; Smalley, R. E. *Nature* **1985**, *318*, 162.
12. Krätschmer, W.; Lamb, L. D.; Fostiropoulos, K.; Huffman, D. R. *Nature* **1990**, *347*, 354.
13. Shinohara, H. *Rep. Prog. Phys.* **2000***, 63,* 843.
14. Watanabe, H.; Inoshita, T. *Optoelectron.–Devices Technol.* **1986**, *1*, 33.
15. Khanna, S. N.; Jena, P. *Phys. Rev. B* **1995**, *51*, 13705.
16. Castleman, A. W.; Khanna, S. N. *J. Phys. Chem. C* **2009**, *113*, 2664.
17. Jena, P. *J. Phys. Chem. Lett.* **2013**, *4*, 1432.
18. Luo, Z.; Castleman, A. W. *Acc. Chem. Res.* **2014**, *47*, 2931.
19. de Heer, W. A. *Rev. Mod. Phys*. **1993**, *65*, 611.
20. Knight, W. D.; Clemenger, K.; de Heer, W. A.; Saunders, W. A.; Chou, M. Y.; Cohen, M. L. *Phys. Rev. Lett.* **1984**, *52*, 2141.
21. Chou, M. Y.; Cleland, A.; Cohen, M. L. *Solid State Commun*. **1984**, *52*, 645.
22. Ekardt, W. *Phys. Rev. B* **1984**, *29*, 1558.
23. Clemenger, K. *Phys. Rev. B* **1985**, *32*, 1359.
24. Katakuse, I.; Ichihara, T.; Fujita, Y.; Matsuo, T.; Sakurai, T.; Matsuda, H. *Int. J. Mass*

Spectrom. Ion Processes **1986**, *74*, 33.

25. Taylor, K. J.; Pettiette-Hall, C. L.; Cheshnovsky, O.; Smalley, R. E. *J. Chem. Phys.* **1992**, *96*, 3319.
26. Chou, M. Y.; Cohen, M. L. *Phys. Lett. A* **1986**, *113*, 420.
27. Taylor, K. J.; Pettiette, C. L.; Craycraft, M. J.; Chesnovsky, O.; Smalley, R. E. *Chem. Phys. Lett.* **1988**, *152*, 347.
28. Martin, T. P.; Bergmann, T.; Göhlich, H.; Lange, T. *J. Phys. Chem.* **1991**, *95*, 6421.
29. Salisbury, B. E.; Wallace, W. T.; Whetten, R. L. *Chem. Phys.* **2000**, *262*, 131.
30. Lee, T. H.; Ervin, K. M. *J. Phys. Chem.* **1994**, *98*, 10023.
31. Wallace, W. T.; Whetten, R. L. *J. Am. Chem. Soc.* **2002**, *124*, 7499.
32. Kim, Y. D.; Fischer, M.; Ganteför, G. *Chem. Phys. Lett.* **2003**, *377*, 170.
33. Vollmer, C.; Janiak, C. *Coordin. Chem. Rev.* **2011**, *255*, 2039.
34. Mafuné, F.; Kohno, J.; Takeda, Y.; Kondow, T.; Sawabe, H. *J. Phys. Chem. B* **2000**, *104*, 9111.
35. Sakamoto, M.; Fujistuka, M.; Majima, T. *J. Photochem. Photobiol. C* **2009**, *10*, 33.
36. Zhang, J.; Ohara, S.; Umetsu, M.; Naka, T.; Hatakeyama, Y.; Adschiri, T. *Adv. Mater.* **2007**, *19*, 203.
37. Jung, J. H.; Oh, H. C.; Noh, H. S.; Ji, J. H.; Kim, S. S. *J. Aerosol Sci.* **2006**, *37*, 1662.
38. Hashimoto, N.; Nishida, N.; Murayama, H.; Tanaka, H. *Chem. Lett.* **2011**, *40*, 144.
39. Qian, H.; Zhu, M.; Wu, Z.; Jin, R. *Acc. Chem. Res.* **2012**, *45*, 1470.
40. Maity, P.; Xie, S.; Yamauchi, M.; Tsukuda, T. *Nanoscale* **2012**, *4*, 4027.
41. Yang, H.; Wang, Y.; Huang, H.; Gell, L.; Lehtovaara, L.; Malola, S.; Häkkinen, H.; Zheng, N. *Nat. Commun*. **2013**, *4*, 2422.
42. Desireddy, A.; Conn, B. E.; Guo, J.; Yoon, B.; Barnett, R. N.; Monahan, B. M.; Kirschbaum, K.; Griffith, W. P.; Whetten, R. L.; Landman, U.; Bigioni, T. P. *Nature* **2013**, *501*, 399.
43. Schulz-Dobrick, M.; Jansen, M. *Z. Anorg. Allg. Chem.* **2007**, *633*, 2326.
44. Briant, C. E.; Theobald, B. R. C.; White, J. W.; Bell, L. K.; Mingos, D. M. P.; Welch, A. J. *J. Chem. Soc., Chem. Commun.* **1981**, 201.
45. Heaven, M. W.; Dass, A.; White, P. S.; Holt, K. M.; Murray, R. W. *J. Am. Chem. Soc.* **2008**, *130*, 3754.
46. Zhu, M; Aikens, C. M.; Hollander, F. J.; Schatz, G. C.; Jin, R. *J. Am. Chem. Soc.* **2008**, *130*, 5883.
47. Pei, Y.; Gao, Y.; Zeng, X. C. *J. Am. Chem. Soc.* **2008**, *130*, 7830.
48. Jadzinsky, P. D.; Calero, G.; Ackerson, C. J.; Bushnell, D. A.; Kornberg, R. D. *Science* **2007**, *318*, 430.

49. Walter, M.; Akola, J.; Lopez-Acevedo, O.; Jadzinsky, P. D.; Calero, G.; Ackerson, C. J.; Whetten, R. L.; Grönbeck, H.; Häkkinen, H. *Proc. Natl. Acad. Sci. U. S. A*. **2008**, *105*, 9157.
50. Akola, J.; Walter, M.; Whetten, R. L.; Häkkinen, H.; Grönbeck, H. *J. Am. Chem. Soc.* **2008**, *130*, 3756.
51. Wang, L. L.; Munir, Z. A.; Maximov, Y. M. *J. Mater. Sci.* **1993**, *28*, 3693.
52. Armstrong, R. W.; Baschung, B.; Booth, D. W.; Samirant, M. *Nano Lett.* **2003**, *3*, 253.
53. Park, K.; Lee, D.; Rai, A.; Mukherjee, D.; Zachariah, M. R. *J. Phys. Chem. B* **2005**, *109*, 7290.
54. Chung, S. W.; Guliants, E. A.; Bunker, C. E.; Hammerstroem, D. W.; Deng, Y.; Burgers, M. A.; Jelliss, P. A.; Buckner, S. W. *Langmuir* **2009**, *25*, 8883.
55. Ghanta, S. R.; Muralidharan, K. *Nanoscale* **2010**, *2*, 976.
56. Lewis, W. K.; Harruff, B. A.; Gord, J. R.; Rosenberger, A. T.; Sexton, T. M.; Guliants, E. A.; Bunker, C. E. *J. Phys. Chem. C* **2011**, *115*, 70.
57. Wu, B.; Liu, X.; Oo, T. Z.; Xing, G.; Mathews, N.; Sum, T. C. *Plasmonics* **2012**, *7*, 677.
58. Chong, X.; Jiang, N.; Zhang, Z.; Roy, S.; Gord, J. R. *J. Nanopart. Res*. **2013**, *15*, 1678.
59. Knight, M. W.; King, N. S.; Liu, L.; Everitt, H. O.; Nordlander, P.; Halas, N. J. *ACS Nano* **2014**, *8*, 834.
60. Viau, G.; Collière, V.; Lacroix, L. M.; Shafeev, G. A. *Chem. Phys. Lett*. **2011**, *501*, 419.
61. Bunker, C. E.; Smith, M. J.; Fernando, K. A. S.; Harruff, B. A.; Lewis, W. K.; Gord, J. R.; Guliants, E. A.; Phelps, D. K. *ACS Appl. Mater. Interfaces* **2010**, *2*, 11.
62. Meziani, M. J.; Bunker, C. E.; Lu, F.; Li, H.; Wang, W.; Guliants, E. A.; Quinn, R. A.; Sun, Y. P. *ACS Appl. Mater. Interfaces* **2009**, *1*, 703.
63. Li, X.; Wu, H.; Wang, X. B.; Wang, L. S. *Phys. Rev. Lett.* **1998**, *81*, 1909.
64. Rao, B. K.; Jena, P. *J. Chem. Phys*. **1999**, *111*, 1890.
65. Leuchtner, R. E.; Harms, A. C.; Castleman, A. W. *J. Chem. Phys*. **1989**, *91*, 2753.
66. Leuchtner, R. E.; Harms, A. C.; Castleman, A. W. *J. Chem. Phys*. **1991**, *94*, 1093.
67. Hettich, R. L. *J. Am. Chem. Soc.* **1989**, *111*, 8582.
68. Cooper, B. T.; Parent, D.; Buckner, S. W. *Chem. Phys. Lett.* **1998**, *284*, 401.
69. Burgert, R.; Schnöckel, H.; Grubisic, A.; Li, X.; Stokes, S. T.; Bowen, K. H.; Ganteför, G. F.; Kiran, B.; Jena, P. *Science* **2008**, *319*, 438.
70. Reber, A. C.; Khanna, S. N.; Roach, P. J.; Woodward, W. H.; Castleman, A. W. *J. Am. Chem. Soc.* **2007**, *129*, 16098.
71. Yuan, Q. H.; Li, J. B.; Fan, X. L.; Lau, W. M.; Liu, Z. F. *Chem. Phys. Lett.* **2010**, *489*, 16.
72. Lu, Q. L.; Chen, L. L.; Wan, J. G.; Wang, G. H. *J. Comput. Chem.* **2010**, *31*, 2804.
73. Neumaier, M.; Olzmann, M.; Kiran, B.; Bowen, K. H.; Eichhorn, B.; Stokes, S. T.;

Buonaugurio, A.; Burgert, R.; Schnöckel, H. *J. Am. Chem. Soc.* **2014**, *136*, 3607.

74. Roach, P. J.; Woodward, W. H.; Castleman, A. W.; Reber, A. C.; Khanna, S. N. *Science* **2009**, *323*, 492.
75. Reber, A. C.; Khanna, S. N.; Roach, P. J.; Woodward, W. H.; Castleman, A. W. *J. Phys. Chem. A* **2010**, *114*, 6071.
76. Reber, A. C.; Roach, P. J.; Woodward, W. H.; Khanna, S. N.; Castleman, A. W. *J. Phys. Chem. A* **2012**, *116*, 8085.
77. Luo, Z.; Smith, J. C.; Woodward, W. H.; Castleman, A. W. *J. Phys. Chem. Lett.* **2012**, *3*, 3818.
78. Bergeron, D. E.; Castleman, A. W.; Morisato, T.; Khanna, S. N. *Science* **2004**, *304*, 84.
79. Grubisic, A.; Li, X.; Ganteför, G.; Bowen, K. H.; Schnöckel, H.; Tenorio, F. J.; Martinez, A. *J. Chem. Phys*. **2009**, *131*, 184305.
80. Dohmeier, C.; Robl, C.; Tacke, M.; Schnöckel, H. *Angew. Chem., Int. Ed.* **1991**, *30*, 564.
81. Purath, A.; Dohmeier, C.; Ecker, A.; Köppe, R.; Krautscheid, H.; Schnöckel, H.; Ahlrichs, R.; Stoermer, C.; Friedrich, J.; Jutzi, P. *J. Am. Chem. Soc.* **2000**, *122*, 6955.
82. Vollet, J.; Hartig, J. R.; Schnöckel, H. *Angew. Chem., Int. Ed.* **2004**, *43*, 3186.
83. Schnöckel, H. *Chem. Rev.* **2010**, *110*, 4125.
84. Clayborne, P. A.; Lopez-Acevedo, O.; Whetten, R. L.; Grönbeck, H.; Häkkinen, H. *Eur. J. Inorg. Chem.* **2011**, 2649.
85. Alnemrat, S.; Hooper, J. P. *J. Chem. Phys*. **2014**, *140*, 104313.
86. Nakajima, A.; Hoshino, K.; Naganuma, T.; Sone, Y.; Kaya, K. *J. Chem. Phys.* **1991**, *95*, 7061.
87. Ko, Y. J.; Shakya, A.; Wang, H.; Grubisic, A.; Zheng, W.; Götz, M.; Ganteför, G.; Bowen, K. H.; Jena, P.; Kiran, B. *J. Chem. Phys.* **2010**, *133*, 124308.
88. Lippa, T. P.; Lyapustina, S. A.; Xu, S. J.; Thomas, O. C.; Bowen, K. H. *Chem. Phys. Lett.* **1999**, *305*, 75.
89. Qiu, L.; Liu, F.; Zhao, L.; Yang, W.; Yao, J. *Langmuir* **2006**, *22*, 4480
90. Tongsakul, D.; Nishimura, S.; Ebitani, K. *J. Phys. Chem. C* **2014**, *118*, 11723.
91. Jiang, P.; Zhou, J. J.; Li, R.; Wang, Z. L.; Xie, S. S. *Nanotechnology* **2006**, *17*, 3533.
92. Tsunoyama, H.; Ichikuni, N.; Sakurai, H.; Tsukuda, T. *J. Am. Chem. Soc*. **2009**, *131*, 7086.
93. Okumura, M.; Kitagawa, Y.; Kawakami, T.; Haruta, M. *Chem. Phys. Lett*. **2008**, *459*, 133.

Chapter 2.

Production of new aluminum oxide clusters having Al_{13} core

Abstract

New aluminum oxide clusters $Al_{14}O^-$ and $Al_{15}O_2^-$ were observed unprecedentedly in the gas-phase reaction of Al_n^- and O_2. Photoelectron spectroscopic measurements and density functional calculations indicated that $Al_{14}O^-$ and $Al_{15}O_2^-$ are composed of an icosahedral Al_{13} moiety bonded by one and two OAl unit(s), respectively. The preferential formation of $Al_{14}O^-$ and $Al_{15}O_2^-$ is explained in terms of the high stability associated with the Al_{13} moiety and efficient collisional trapping as intermediates of oxidative etching reactions.

2.1 Introduction

Aluminum is known to react readily with oxygen (O_2) while releasing a huge amount of heat. By taking advantage of this feature, Al powders have been used as additives in propellants, explosives and fuels.[1] Recent studies have demonstrated that the combustion rates of Al particles increased significantly with a decrease in diameter down to few tens of nanometers.[1–6] Several efforts have been made to synthesize Al nanoparticles resistant to oxidation and to apply them as energetic materials.[4–6] Atomic-level understanding has been obtained for the oxidation of much smaller Al clusters through the pioneering works of Castleman and co-workers.[7,8] Aluminum cluster cations and anions are etched into smaller clusters during the oxidation, corresponding to the combustion of Al powders. For Al cluster anions, the following reaction paths are well established.[7,9]

$$Al_n^- + O_2 \rightarrow Al_{n-1}O + AlO^- \text{ or } Al_{n-1} + AlO_2^- \ (n \leq 7) \quad (2.1)$$

$$Al_n^- + O_2 \rightarrow Al_{n-4}^- + 2Al_2O \quad (n \geq 8) \quad (2.2)$$

Interestingly, magic clusters such as Al_7^+, Al_{13}^-, and Al_{23}^- showed high tolerance for O_2[7,10] in contrast to the efficient oxidation of Al nanoparticles. Such inertness toward O_2 has been attributed to the closure of electronic shells for the clusters (20, 40, and 70 valence electrons, respectively).[11–15] Theoretical studies have shown that this chemical inertness is due to the barrier required for transition of the spin states from triplet intermediates to singlet products in $^1Al_{13}^- + {}^3O_2 \rightarrow {}^3[Al_{13}{\cdot}O_2]^- \rightarrow {}^1Al_9^- + 2Al_2O$.[16–18]

In this chapter, chemical reactions of Al_n^- under high-pressure O_2 were investigated to gain insights into the stability of Al_{13}^- under atmospheric conditions. As a result, new products, $Al_{14}O^-$ and $Al_{15}O_2^-$, were observed. The electronic and geometrical structures of these new aluminum oxides were examined using

photoelectron spectroscopy and density functional theory (DFT) calculations. The mechanism of the preferential formation of $Al_{14}O^-$ and $Al_{15}O_2^-$ is also discussed.

2.2 Experimental and computational method

2.2.1 Experimental method

The experimental apparatus used in the present study was composed of a cluster source, reaction cell, time-of-flight (TOF) mass spectrometer, and magnetic bottle-type photoelectron spectrometer (Figure 2.1).[19] Experiments were performed at 10 Hz, and all the pulse sequences described below were controlled by digital delay generators (Standard Research Systems, DG645). The vacuum chamber was differentially pumped by three turbo molecular pumps at the pumping speeds shown in Figure 2.1. Pressure of the source chamber increased from 2×10^{-5} to 4×10^{-3} Pa under the typical experimental conditions. The pressure of the photodetachment chamber was kept below 1×10^{-5} Pa during the measurement.

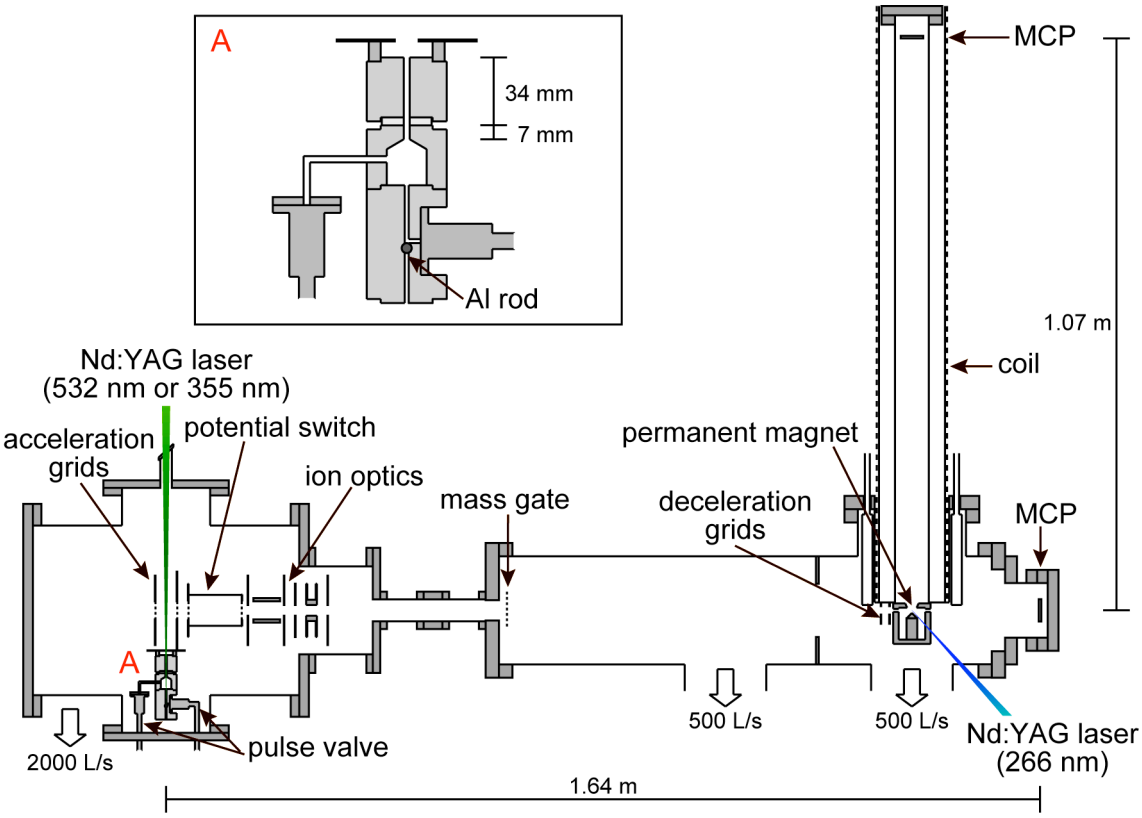

Figure 2.1. Schematic of the experimental apparatus. Inset shows an expanded view of part A.

Generation of Al cluster was conducted by laser vaporization method.[20] First, an Al target rod (99.99%; ϕ = 5 mm; L = 22 mm) with rotating and translating motion was irradiated by a focused output of the second or third harmonics of a Nd:YAG laser (Spectra-Physics, INDI-HG) 10–50 mJ/pulse. Then, helium gas (99.995%) with a backing pressure of 4–8 atm was injected into the channel (L = 28 mm) to produce Al clusters by opening a pulse valve with orifice 0.8 mm in diameter (Parker Hannifin, series 9) for 200–250 μs. The Al cluster anions produced were allowed to react with O_2 (2 atm; purity 99.5%), which was introduced into the reaction cell through a pulse valve. After passing through a channel (ϕ = 3 mm and L = 7 or 41 mm), the unreacted parent clusters and reaction products were expanded into the source chamber and were

extracted perpendicularly by applying a pulsed electric field at about 75 mm downstream the exit of the nozzle. The anions were accelerated to 2.3–5.8 keV, steered by deflectors and an einzel lens, and detected by a microchannel plate (El-Mul, Double MCP 33) located at 1.64 m. The ion signals were recorded using a digital oscilloscope (Tectronix, TDS 580D). Typical resolution of the TOF mass spectrometer was ~150.

The photoelectron spectra of the parent Al anions and the products at a kinetic energy of 2.3 keV were recorded by irradiating the fourth harmonic of a Nd:YAG laser (Spectra-Physics, INDI-40) with < 5 mJ/pulse. The detachment laser was polarized to parallel with respect to the flight path of the ions. The photoelectrons ejected from the cluster anions were collected by a strong magnetic field (~1000 G) produced by a permanent magnet and guided by a weak field (~10 G) produced by a solenoid coil to a microchannel plate (El-Mul, Double MCP 33) located at 1.07 m. The signals were amplified by preamplifier (Standard Research Systems, SR445A) and counted using a multichannel scaler (Standard Research Systems, SR430) with a time bin of 5 ns. The time-dependent photoelectron spectra were converted to energy-dependent spectra by considering the Jacobian factor. The photoelectron spectra accumulated for 10,000–65,000 laser shots were presented after subtracting the background spectra. The electron energy was calibrated using the photoelectron spectrum of I^- after deceleration using a momentum decelerator;[21] I^- was produced by dissociative electron attachment to CH_3I. Typical photoelectron spectra recorded for Al_n^- ($12 \leq n \leq 16$) are shown in Figure 2.2, which reproduced previous results.[11–15] Although the resolution of the photoelectron spectrometer was not high (230 meV for electrons with a kinetic energy of 0.66 eV), this does not affect the discussion.

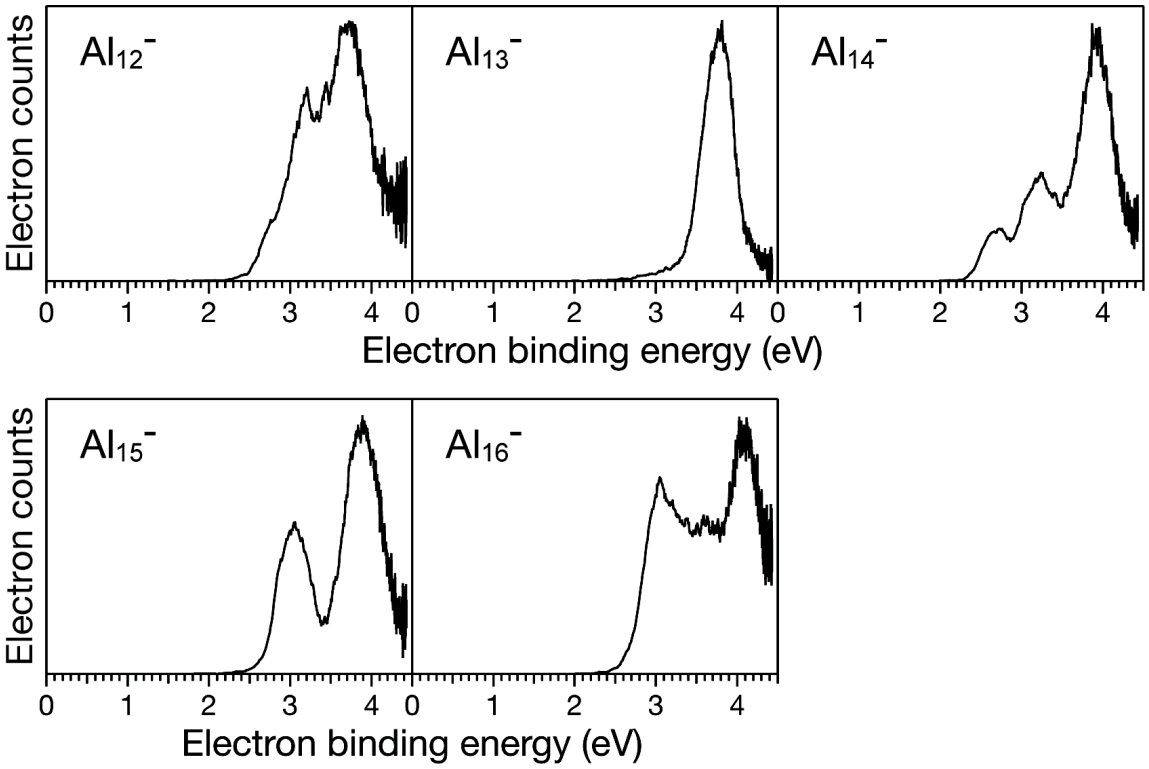

Figure 2.2. Photoelectron spectra of Al_n^- ($12 \leq n \leq 16$).

2.2.2 Computational method

Electronic and geometrical structures of $Al_{14}O^-$, $Al_{15}O_2^-$, and Al_n^- ($12 \leq n \leq 16$) were calculated by DFT at the B3LYP level with the 6-31G(d) basis set[22] using the Gaussian 09 package.[23] Stability of the optimized clusters was confirmed by analyzing the vibrational frequencies. The vertical detachment energy (VDE) was calculated as the energy difference between the ground state of the anion and that of the neutral cluster with the geometry of the anion. The structures and VDE values of Al_n^- ($12 \leq n \leq 16$) calculated at the same level of theory are summarized in Figure 2.3 and Table 2.1, respectively. The results are in good agreement with those reported previously.[14,15]

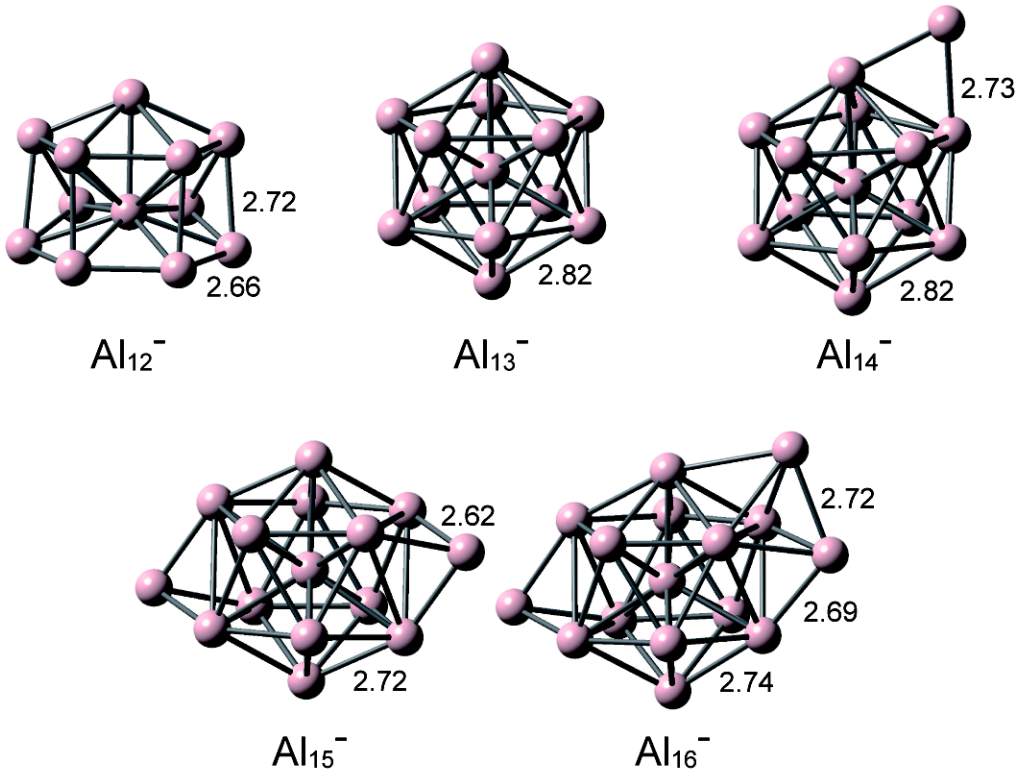

Figure 2.3. Optimized structures of Al_n^- ($12 \leq n \leq 16$) obtained at the B3LYP/6-31G(d) level.

Table 2.1. VDE of Al_n^- ($12 \leq n \leq 16$).

n	VDE_{cal} (eV)[a]	VDE_{exp} (eV)[b]
12	2.43	2.80 ± 0.1
13	3.45	3.75 ± 0.1
14	2.59	2.65 ± 0.1
15	2.81	2.95 ± 0.1
16	2.80	

[a]Calculated for the structures shown in Figure 2.3 at the B3LYP/6-31G(d) level. [b]From ref 12.

2.3 Results and discussion

2.3.1 Generation of Al cluster anions

Figure 2.4 shows typical mass spectrum of Al cluster anions that was measured by the apparatus shown in Figure 2.1. As described above,[7–10,16] Al_{13}^- and Al_{23}^- were abundant species, reflecting its stability as compared with its neighbors.

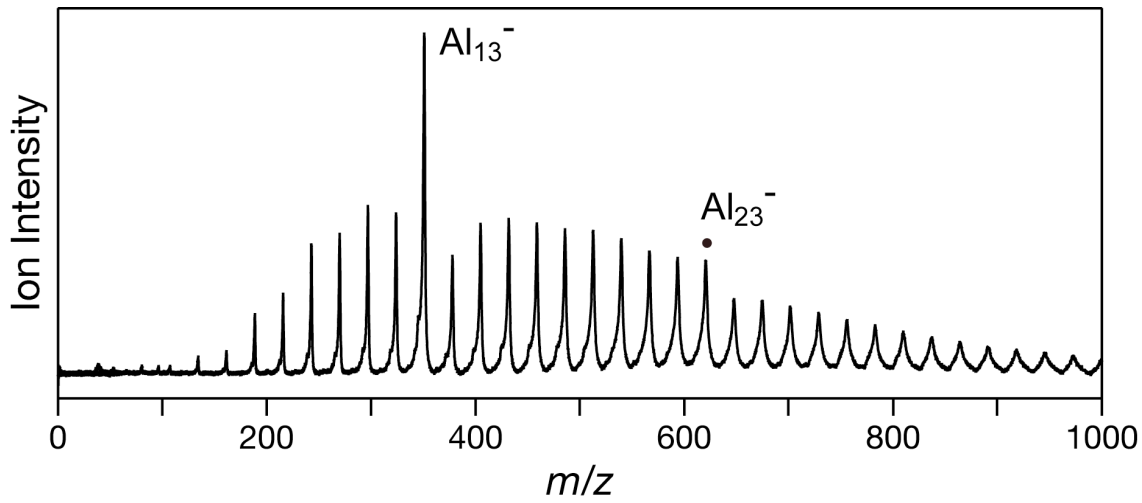

Figure 2.4. Typical mass spectrum of Al cluster anions.

2.3.2 Formation of unprecedented products

Figures 2.5(a) and 2.5(b) show portions of the mass spectra of Al cluster anions before and after reaction with O_2, respectively. After reaction with O_2 (Figure 2.5(b)), the intensity of Al_{13}^- remained unchanged, whereas those of other species decreased significantly. In addition, aluminum oxide species, AlO^- and AlO_2^-, were generated. These results can be explained by the oxidative etching reactions of Al_n^- (Eqs. 2.1 and 2.2)[9] and the high tolerance of Al_{13}^-.[7,10] Interestingly, two new types of aluminum oxide clusters, Al_nO^- and $Al_mO_2^-$, were observed from the cluster source.

Among each series, $Al_{14}O^-$ and $Al_{15}O_2^-$ showed extraordinarily high abundance. The $Al_{14}O^-$ and $Al_{15}O_2^-$ species have not been reported previously although aluminum-rich oxide clusters (Al_nO and Al_mO_2) have been studied extensively.[24–27] This discovery is attributable to a setup of the reaction cell (Figure 2.1); the production of $Al_{14}O^-$ and $Al_{15}O_2^-$ was almost completely suppressed when the length of the channel after the reaction cell was reduced from 41 to 7 mm (Figure 2.6).

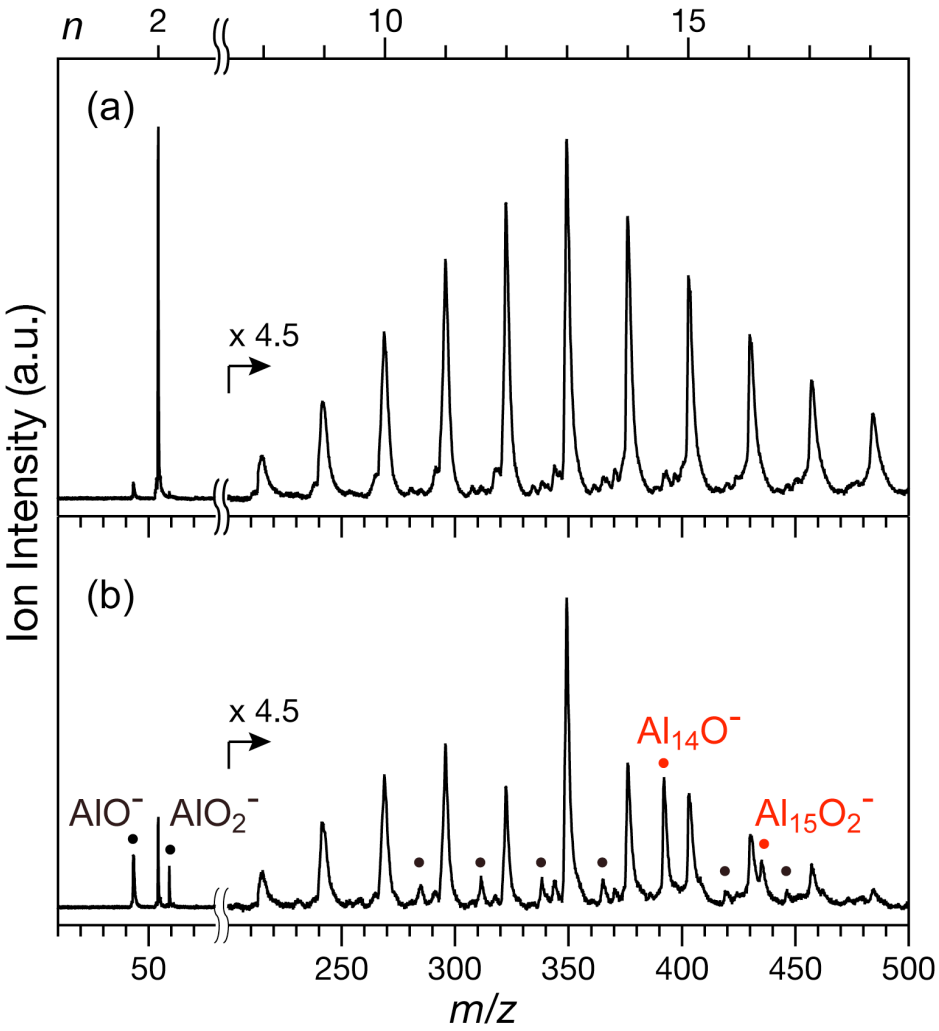

Figure 2.5. Mass spectra of Al_n^- (a) before and (b) after reaction with O_2.

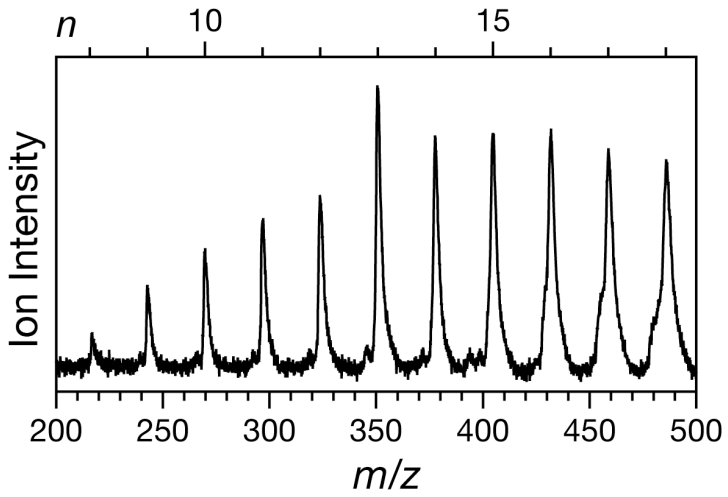

Figure 2.6. Mass spectrum of Al_n^- with O_2 with a channel length of 7 mm.

2.3.3 Photoelectron spectra

Figure 2.7 shows photoelectron spectra of $Al_{14}O^-$ and $Al_{15}O_2^-$ recorded with 266 nm photons. The spectra of $Al_{14}O^-$ and $Al_{15}O_2^-$ exhibited asymmetrical bell-shaped profiles. The "apparent" VDE values, defined as the energy giving the peak top, of $Al_{14}O^-$ and $Al_{15}O_2^-$ were determined to be 3.86 ± 0.02 and 3.93 ± 0.02 eV, respectively, by fitting the data with fourth-order polynomials.

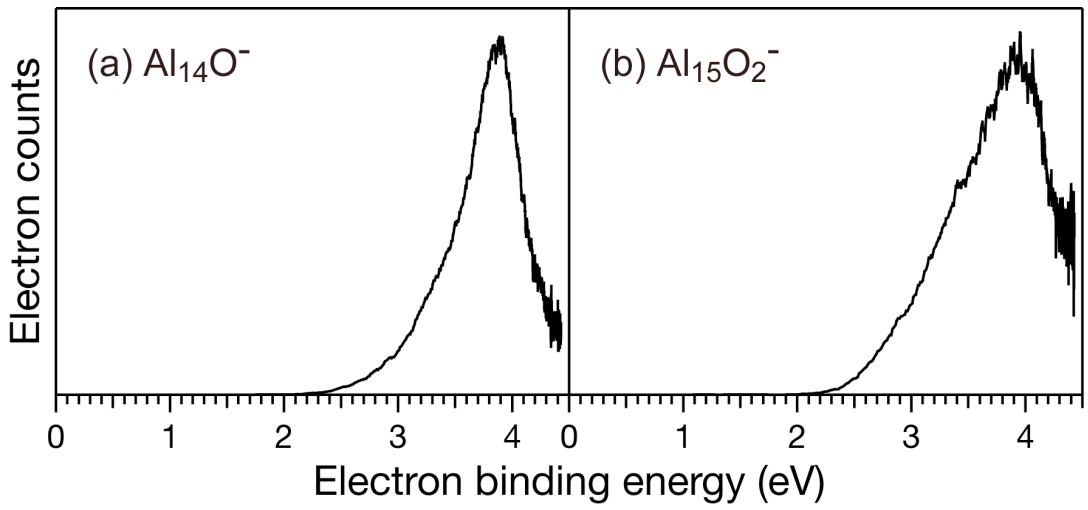

Figure 2.7. Photoelectron spectra of (a) $Al_{14}O^-$ and (b) $Al_{15}O_2^-$.

2.3.4 Computational results

The geometrical structures of the new products were studied by DFT calculations (B3LYP/6-31G(d)). For the structural optimization of $Al_{14}O^-$, initial structures that contained an OAl unit bonded to icosahedral Al_{13}, either through an O or Al site, were considered. Isomers **1**, **2**, and **3** were obtained by optimization of initial structures in which the O atom of the OAl unit is bonded to an atop, a bridge, or a hollow site of the Al_{13}, respectively (Figure 2.8). In isomer **1**, the icosahedral motif of the Al_{13} moiety was retained. The bond lengths of Al–O and Al_{13}–O were 1.70 and 1.75 Å, respectively. In isomer **2**, the icosahedral Al_{13} core was deformed into a decahedral motif, and the OAl unit was bonded on a tilt. In isomer **3**, the O atom is bonded to the bridged site of the deformed Al_{13} core. In contrast, optimization of initial structures in which the Al atom of the OAl unit is bonded to the atop site of icosahedral Al_{13} yielded isomer **4**, whereas isomer **5** was obtained from those in which the OAl unit is bonded to the bridge and hollow sites of Al_{13} (Figure 2.8). In isomers **4** and **5**, the OAl unit was bonded to the icosahedral Al_{13} moiety in an upright configuration.

Relative stability and VDE values of isomers **1** – **5** are compared in Table 2.2. Isomers **1** – **3**, which contain OAl bound to Al_{13} through an O–Al bond, were significantly more stable than **4** and **5**, which contained the OAl bound to Al_{13} through an Al–Al bond. A bonding motif similar to **1** – **3** was theoretically predicted for smaller, neutral Al_nO clusters ($n \leq 10$).[26] In addition, the VDE value of **1** was 3.27 eV, which is slightly less than the experimental value (3.86 eV), whereas those of **2** and **3** were ~2.4 eV, which is significantly less than the experimental value.

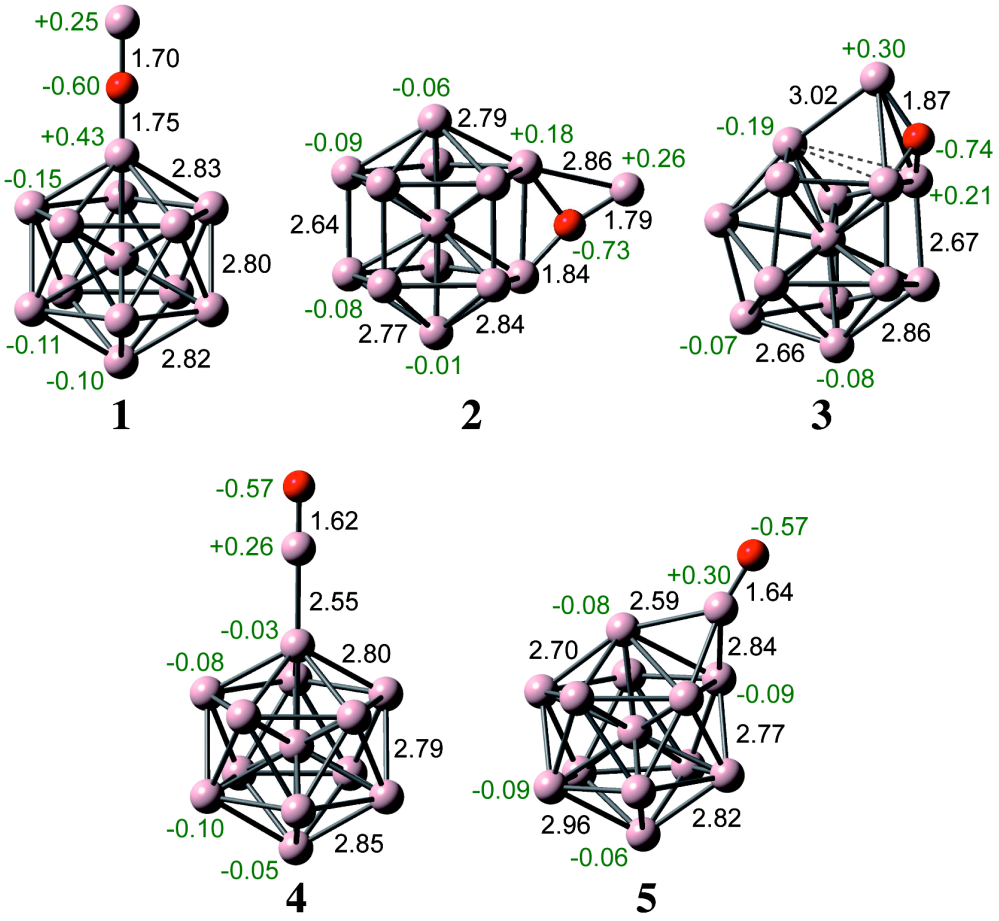

Figure 2.8. Optimized structures of isomers (**1** – **5**) of $Al_{14}O^-$ obtained at B3LYP/6-31G(d). The oxygen atoms are shown in red. Black and green numbers represent selected bond lengths (Å) and Mulliken charges, respectively.

Table 2.2. ΔE and VDE of $Al_{14}O^-$ Obtained at B3LYP/6-31G(d).

isomer	state	symmetry	ΔE (eV)	VDE (eV)[a]
1	$^2A_1$	C_{5v}	0.00	3.27[b]
2	^2A	C_1	0.65	2.38
3	^2A	C_1	0.52	2.40
4	^2A	C_1	1.93	3.39
5	^2A	C_1	1.79	2.78

[a]Experimental value: 3.86 ± 0.02 eV. [b]3.31 eV at B3LYP/6-31+G(d).

An extensive survey to identify the most stable structure of $Al_{14}O^-$ suggested that $Al_{15}O_2^-$ is constructed by two OAl units bonded to the atop sites of icosahedral Al_{13} through the O site. Three isomers (**6** – **8**) were obtained from initial structures, in which two OAl units were bonded to two sites of Al_{13}^- in the para, meta, and ortho positions, respectively (Figure 2.9). In isomer **6**, the Al_{13} core retained the icosahedral motif, whereas it was strongly distorted by the two AlO units bonded in **7** and **8**. Table 2.3 lists the relative stability and VDE values of **6** – **8**. Isomer **6** is most stable among the three isomers, and its VDE value (3.28 eV) is most close to the experimental value (3.93 eV).

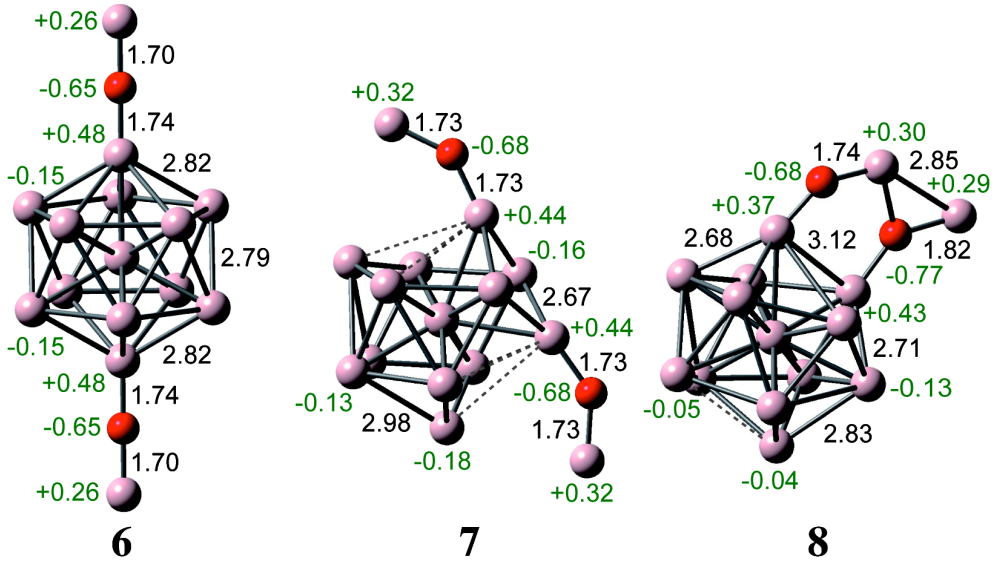

Figure 2.9. Optimized structures of isomers (**6** – **8**) of $Al_{15}O_2^-$ obtained at B3LYP/6-31G(d). The oxygen atoms are shown in red. Black and green numbers represent selected bond lengths (Å) and Mulliken charges, respectively.

Table 2.3. ΔE and VDE of $Al_{15}O_2^-$ Obtained at B3LYP/6-31G(d).

isomers	state	symmetry	ΔE (eV)	VDE (eV)[a]
6	$^1A_{1g}$	D_{5d}	0.00	3.28[b]
7	^1A	C_1	0.91	2.88
8	^1A	C_1	0.43	3.16

[a]Experimental value: 3.93 ± 0.02 eV. [b]3.31 eV at B3LYP/6-31+G(d).

2.3.5 Structures of $Al_{14}O^-$ and $Al_{15}O_2^-$

Relative stability between five isomers of $Al_{14}O^-$ (Table 2.2) indicates that isomers **1** – **3** are potential candidates. Among **1** – **3**, the VDE value calculated for **1** is the closest to that of experimental value. Underestimation of the VDE value is also

found in the calculation of Al_{12}^-–Al_{16}^- at the same level of theory (Table 2.1); the calculated values are smaller than the experimental values[11–15] by 0.06–0.37 eV. Comparison of the stability and VDE values indicates that isomer **1** represents the most probable structure of new product $Al_{14}O^-$. Similar discussion based in Table 2.3 leads us to conclude that isomer **6** is the most plausible candidate for $Al_{15}O_2^-$. I therefore conclude that the aluminum oxide anions, $Al_{14}O^-$ and $Al_{15}O_2^-$, are constructed by bonding one and two OAl units to the icosahedral Al_{13} core, respectively. These structures remind us of superatom cluster compounds composed of Al_{13} moieties.[28–31]

The bonding scheme between the OAl unit and Al_{13} in $Al_{14}O^-$ (**1**) was examined using the shape of the frontier molecular orbitals. Figure 2.10(d) shows a singly occupied molecular orbital (SOMO) of $Al_{14}O^-$, which had a doublet electronic configuration. This orbital is constructed via antibonding interaction between the SOMO of AlO (Figure 2.10(b)) and the HOMO-1 of Al_{13}^- (Figure 2.10(a)), which is lower in energy than its highest occupied molecular orbital (HOMO). In contrast, the bonding interaction between the SOMO of AlO and the HOMO-1 of Al_{13}^- creates the HOMO-5 of $Al_{14}O^-$ (Figure 2.10(c)). Accommodation of two electrons into the HOMO-5 is the origin of strong bonding between AlO and Al_{13}^- in $Al_{14}O^-$.

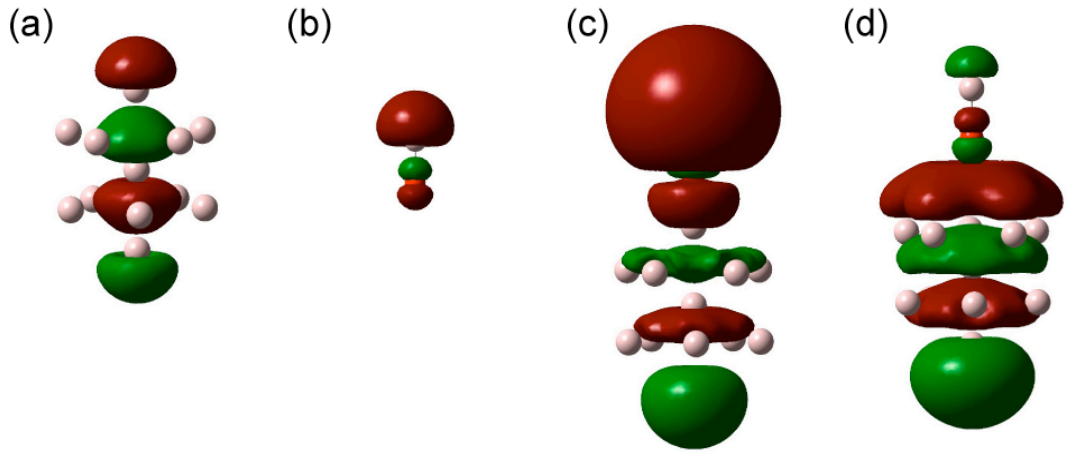

Figure 2.10. Charge-density surfaces of (a) HOMO-1 of Al_{13}^-, (b) SOMO of AlO, (c) HOMO-5 and (d) SOMO of $Al_{14}O^-$ (**1**). The isodensity values are (a) 0.03 e, (b) 0.05 e, (c) 0.07 e, and (d) 0.015 e.

2.3.6 Preferential formation of $Al_{14}O^-$ and $Al_{15}O_2^-$

The question is why are the $Al_{14}O^-$ and $Al_{15}O_2^-$ ions formed preferentially under the present experimental conditions. It is known that reaction of Al_n^- ($n \geq 8$) with O_2 proceeds exclusively by releasing a highly stable fragment Al_2O (Eq. 2.2).[9] In the framework of this reaction path, $Al_{14}O^-$ and $Al_{15}O_2^-$ correspond to intermediates of oxidative etching reactions of Al_{16}^- and Al_{15}^-, respectively.[32] DFT calculations (B3LYP/6-31G(d)) were conducted to estimate enthalpies of the formation of $Al_{14}O^-$ and $Al_{15}O_2^-$ from Al_{16}^- and Al_{15}^- and for the removal of Al_2O. The optimized structures and enthalpies of the formation of the relevant species are shown in Figures 2.3 and 2.11 and Table 2.4. The formation of $Al_{14}O^-$ from Al_{16}^- was exothermic by 7.46 eV, whereas removal of Al_2O from $Al_{14}O^-$ was endothermic by 1.78 eV (Figure 2.12). The formation of $Al_{15}O_2^-$ from Al_{15}^- was exothermic by 11.72 eV, whereas the removal of Al_2O from $Al_{15}O_2^-$ was endothermic by 1.92 eV (Figure 2.12). These energetic

considerations support that $Al_{14}O^-$ and $Al_{15}O_2^-$ correspond to stable intermediates of the consecutive etching reactions because of the high stability of the icosahedral Al_{13} moiety. The observation of these previously unreported species is ascribed to efficient collisional stabilization in the reaction cell used in this study.

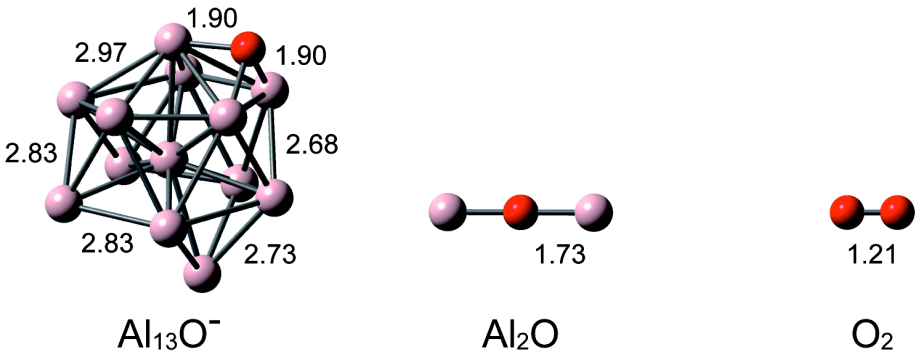

Figure 2.11. Optimized structures of $Al_{13}O^-$, Al_2O and O_2 obtained at the B3LYP/6-31G(d) level. The numbers are selected bond lengths (Å).

Table 2.4. Total Energy of O_2 and $Al_nO_m^-$.

	E (Hartree)[a]
O_2	–150.3200421
Al_2O	–560.1798515
Al_{12}^-	–2909.3725651
$Al_{13}O^-$	–3227.1492532
$Al_{14}O^-$	–3469.6178843
Al_{15}^-	–3636.7520577
$Al_{15}O_2^-$	–3787.3998384
Al_{16}^-	–3879.2035060

[a]Calculated for the structures shown in Figures 2.3, 2.8, 2.9, and 2.11 at the B3LYP/6-31G(d) level.

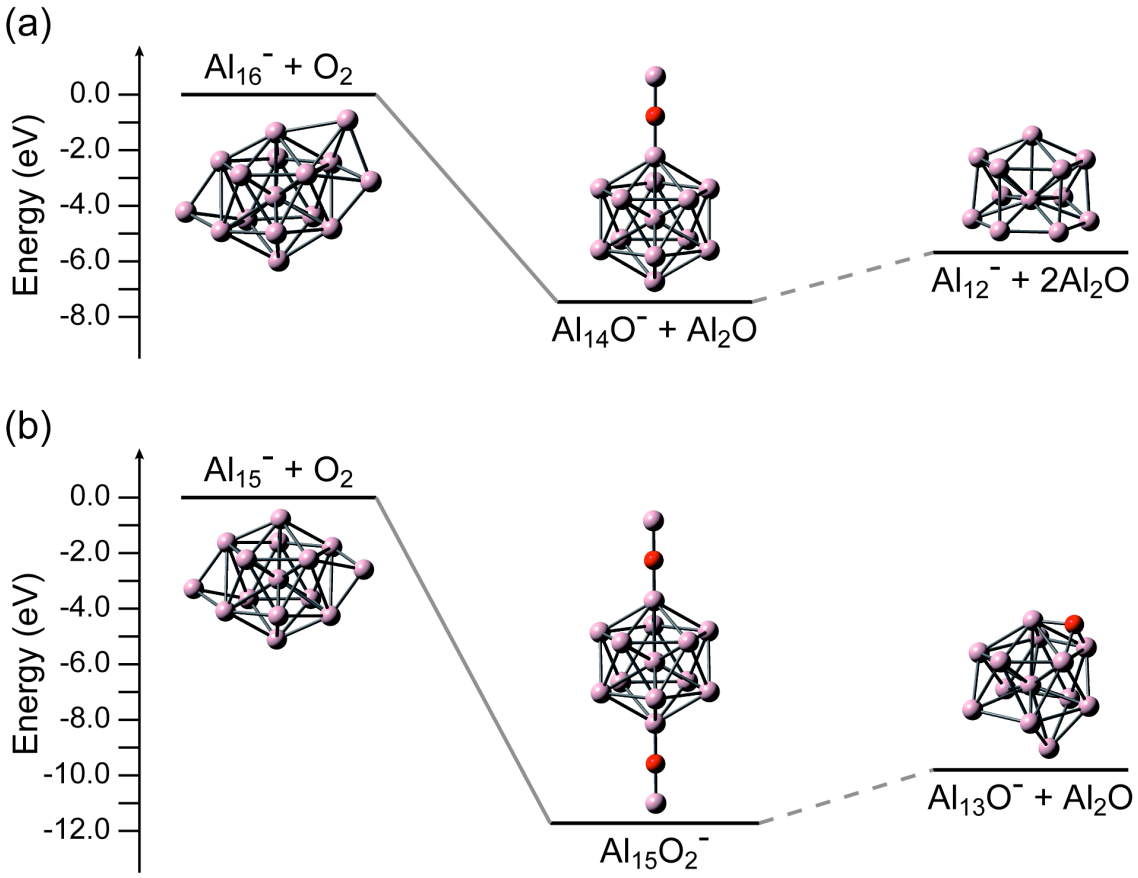

Figure 2.12. Energy diagrams of production processes of (a) $Al_{14}O^-$ and (b) $Al_{15}O_2^-$.

2.4 Conclusion

In summary, reaction of Al_n^- and O_2 under a high-pressure condition yielded the previously unknown aluminum oxides $Al_{14}O^-$ and $Al_{15}O_2^-$. Photoelectron spectroscopy and density functional calculations revealed that $Al_{14}O^-$ and $Al_{15}O_2^-$ are composed of an icosahedral Al_{13} moiety bonded by one and two OAl unit(s), respectively. The preferential formation of $Al_{14}O^-$ and $Al_{15}O_2^-$ was due to their high stability associated with the Al_{13} moiety and the efficient dissipation of reaction exothermicity by collisional cooling. The present findings suggest that these Al oxide clusters with an icosahedral Al_{13} moiety are potential candidates for energetic materials

stable against oxidation without protecting layers.

References

1. Wang, L. L.; Munir, Z. A.; Maximov, Y. M. *J. Mater. Sci.* **1993**, *28*, 3693.
2. Armstrong, R. W.; Baschung, B.; Booth, D. W.; Samirant, M. *Nano Lett.* **2003**, *3*, 253.
3. Park, K.; Lee, D.; Rai, A.; Mukherjee, D.; Zachariah, M. R. *J. Phys. Chem. B* **2005**, *109*, 7290.
4. Chung, S. W.; Guliants, E. A.; Bunker, C. E.; Hammerstroem, D. W.; Deng, Y.; Burgers, M. A.; Jelliss, P. A.; Buckner, S. W. *Langmuir* **2009**, *25*, 8883.
5. Ghanta, S. R.; Muralidharan, K. *Nanoscale* **2010**, *2*, 976.
6. Lewis, W. K.; Harruff, B. A.; Gord, J. R.; Rosenberger, A. T.; Sexton, T. M.; Guliants, E. A.; Bunker, C. E. *J. Phys. Chem. C* **2011**, *115*, 70.
7. Leuchtner, R. E.; Harms, A. C.; Castleman, A. W. *J. Chem. Phys*. **1989**, *91*, 2753.
8. Leuchtner, R. E.; Harms, A. C.; Castleman, A. W. *J. Chem. Phys*. **1991**, *94*, 1093.
9. Cooper, B. T.; Parent, D.; Buckner, S. W. *Chem. Phys. Lett.* **1998**, *284*, 401.
10. Hettich, R. L. *J. Am. Chem. Soc.* **1989**, *111*, 8582.
11. Taylor, K. J.; Pettiette, C. L.; Craycraft, M. J.; Chesnovsky, O.; Smalley, R. E. *Chem. Phys. Lett.* **1988**, *152*, 347.
12. Cha, C. Y.; Ganteför, G.; Eberhardt, W. *J. Chem. Phys.* **1994**, *100*, 995.
13. Li, X.; Wu, H.; Wang, X. B.; Wang, L. S. *Phys. Rev. Lett.* **1998**, *81*, 1909.
14. Akola, J.; Manninen, M.; Häkkinen, H.; Landman, U.; Li, X.; Wang, L. S. *Phys. Rev. B* **1999**, *60*, 11297.
15. Ma, L.; von Issendorff, B.; Aguado, A. *J. Chem. Phys.* **2010**, *132,* 104303.
16. Burgert, R.; Schnöckel, H.; Grubisic, A.; Li, X.; Stokes, S. T.; Bowen, K. H.; Ganteför, G. F.; Kiran, B.; Jena, P. *Science* **2008**, *319*, 438.
17. Yuan, Q. H.; Li, J. B.; Fan, X. L.; Lau, W. M.; Liu, Z. F. *Chem. Phys. Lett.* **2010**, *489*, 16.
18. Lu, Q. L.; Chen, L. L.; Wan, J. G.; Wang, G. H. *J. Comput. Chem.* **2010**, *31*, 2804.
19. Tsukuda, T.; Saeki, M.; Iwata, S.; Nagata, T. *J. Phys. Chem. A* **1997**, *101*, 5103.
20. Dietz, T. G.; Duncan, M. A.; Powers, D. E.; Smalley, R. E. *J. Chem. Phys.* **1981**, *74*, 6511.
21. Wang, L. S.; Cheng, H. S.; Fan, J. *J. Chem. Phys.* **1995**, *102*, 9480.
22. The VDE values of Al_{13}^- calculated at various basis sets were comparable: 3.45 eV (6–31G(d)); 3.47 eV (6–31+G(d)); 3.46 eV (6–311G(d)); 3.46 eV (6–311+G(d)).
23. Frisch, M. J.; Trucks, G. W.; Schlegel, H. B.; Scuseria, G. E.; Robb, M. A.; Cheeseman, J. R.; Scalmani, G.; Barone, V.; Mennucci, B.; Petersson, G. A.; Nakatsuji, H.; Caricato, M.; Li, X.; Hratchian, H. P.; Izmaylov, A. F.; Bloino, J.; Zheng, G.; Sonnenberg, J. L.; Hada, M.; Ehara, M.; Toyota, K.; Fukuda, R.; Hasegawa, J.; Ishida, M.; Nakajima, T.; Honda, Y.; Kitao, O.; Nakai, H.; Vreven, T.; Montgomery, J. A., Jr.; Peralta, J. E.; Ogliaro, F.;

Bearpark, M.; Heyd, J. J.; Brothers, E.; Kudin, K. N.; Staroverov, V. N.; Keith, T.; Kobayashi, R.; Normand, J.; Raghavachari, K.; Rendell, A.; Burant, J. C.; Iyengar, S. S.; Tomasi, J.; Cossi, M.; Rega, N.; Millam, J. M.; Klene, M.; Knox, J. E.; Cross, J. B.; Bakken, V.; Adamo, C.; Jaramillo, J.; Gomperts, R.; Stratmann, R. E.; Yazyev, O.; Austin, A. J.; Cammi, R.; Pomelli, C.; Ochterski, J. W.; Martin, R. L.; Morokuma, K.; Zakrzewski, V. G.; Voth, G. A.; Salvador, P.; Dannenberg, J. J.; Dapprich, S.; Daniels, A. D.; Farkas, O.; Foresman, J. B.; Ortiz, J. V.; Cioslowski, J.; Fox, D. J. *Gaussian 09*, *Revision C.01*, Gaussian, Inc., Wallingford CT, 2010.

24. Wu, H.; Li, X.; Wang, X. B.; Ding, C. F.; Wang, L. S. *J. Chem. Phys.* **1998**, *109*, 449.
25. Martínez, A.; Sansores, L. E.; Salcedo, R.; Tenorio, F. J.; Ortiz, J. V. *J. Phys. Chem. A* **2002**, *106*, 10630.
26. Sun, J.; Lu, W. C.; Wang, H.; Li, Z. S.; Sun, C. C. *J. Phys. Chem. A* **2006**, *110*, 2729.
27. Neukermans, S.; Veldeman, N.; Janssens, E.; Lievens, P.; Chen, Z.; Schleyer, P. v. R. *Eur. Phys. J. D* **2007**, *45*, 301.
28. Bergeron, D. E.; Castleman, A. W.; Morisato, T.; Khanna, S. N. *Science* **2004**, *304*, 84.
29. Bergeron, D. E.; Castleman, A. W.; Morisato, T.; Khanna, S. N. *J. Chem. Phys.* **2004**, *121*, 10456.
30. Bergeron, D. E.; Roach, P. J.; Castleman, A. W.; Jones, N. O.; Khanna, S. N. *Science* **2005**, *307*, 231.
31. Akutsu, M.; Koyasu, K.; Atobe, J.; Hosoya, N.; Miyajima, K.; Mitsui, M.; Nakajima, A. *J. Phys. Chem. A* **2006**, *110*, 12073.
32. In our beam condition, production of Al_{16}^- and Al_{15}^- from Al_{20}^- and Al_{19}^- by oxidative etching, respectively, is negligible.

Chapter 3.

Stabilization of Al_{13} by electron donating ligand

Abstract

The sequential bonding of *N*-ethyl-2-pyrrolidone (EP), a monomer unit of poly(vinylpyrrolidone) (PVP), to an open-shell superatom Al_{13} was studied by density functional theory calculations. The first three EP ligands prefer to be chemisorbed on the atop sites of Al_{13} via the carbonyl O atom mainly due to bonding interaction between molecular orbitals of EP and the 1S or 1D superatomic orbital of Al_{13}.The fourth EP ligand, however, prefers to be bound electrostatically to one of the chemisorbed EP ligands rather than to be chemisorbed on Al_{13}. This behavior suggests that maximum number of PVP that can be chemisorbed on an Al cluster is determined not only by the steric repulsion between adjacent PVP but also by the electronic charge accumulated on the Al cluster. The gross Mulliken charge accumulated on the Al_{13} moiety increases with the number of EP ligands chemisorbed and reaches nearly –1 e in $Al_{13}(EP)_3$, suggesting the closure of the electronic shell of Al_{13} by ligation of three EP ligands. However, the spin density analysis revealed that the superatomic orbital 1F of Al_{13} remains singly occupied even after chemisorption of three EP ligands. In conclusion, the Al_{13} moiety stabilized by PVP remains to be an open-shell superatom although it accepts electronic charge through polarized Al–O bonding.

3.1 Introduction

Nanoparticles and clusters of aluminum that are stable under ambient conditions have gained current interest as energetic materials,[1–3] optical devices,[4,5] and hydrogen storage materials.[6,7] To prevent oxidation of the surface and aggregation, Al nanoparticles are passivated by organic reagents, such as poly(vinylpyrrolidone) (PVP), poly(methylmethacrylate), oleic acid, and isophthalic acid or embedded in matrices of ammonium nitrate and ammonium perchlorate. In contrast, small ligands such as pentamethylcyclopentadienyl (Cp*) have been used to synthesize atomically precise Al clusters including $Al_4Cp^*_4$, $Al_8Cp^*_4$, and $Al_{50}Cp^*_{12}$.[8] In these examples, the ligands act not only to sterically protect the clusters from aggregation but also to electronically stabilize the clusters by adjusting the formal number of the valence electrons confined in the clusters (n^*). The n^* values of the above clusters are calculated to be 8, 20, and 138, respectively, according to a simple scheme[9] developed to explain the electronic stability of the ligand-protected Au clusters. In the calculation, it is assumed that each Al atom provides three valence electrons due to the hybridization of 3s and 3p orbitals[10] and that each Cp* ligand takes one electron from the Al clusters.[11] These n^* values agree with those predicted from the electronic shell model for spherical clusters of simple metals (Au, Na, Al).[12] According to the electronic shell model, the clusters gain high stability due to closure of the superatomic orbitals (1S, 1P, 1D, 2S, 1F, 2P, 1G, 2D, 3S, 1H, ...) when n^* adopts values of 2, 8, 18, 20, 34, 40, 58, 68, 70, 92, and so on.[13] The above consideration suggests high stability of the above Cp*-protected Al clusters in terms of electronic structure. However, they are easily oxidized in air although it was theoretically shown that the oxidation rates are retarded by employing Cp* as compared with the less bulky cyclopentadienyl ligand.[14]

Other potential candidates for air-stable Al clusters are magic Al clusters such as Al_{13}^- and Al_{23}^- anions[12] which are known to be stable against oxygen,[15] water,[16] and methanol.[17] The high stability of Al_{13}^- against O_2 is ascribed to a perfect icosahedral geometrical structure, closed electronic shell with a configuration of $(1S)^2(1P)^6(1D)^{10}(2S)^2(1F)^{14}(2P)^6$, and high energy barrier associated with spin conversion.[18] Now the challenge to producing Al_{13}^- is how we can externally supply one extra electron to open-shell Al_{13}. The simplest way of supplying one electron to Al_{13} is to dope an alkali metal atom[19] as demonstrated by the formation of $Al_{13}X$ (X = H, Au, and alkali metals)[19,20] in the gas phase.

In this chapter, I examined a stabilization of Al_{13} by an electron-donating ligand, with PVP as a candidate: it has been demonstrated experimentally that Pt clusters[21–23] and Au clusters[24,25] stabilized by PVP are negatively charged. It has also been shown theoretically that PVP donates electronic charge to Au_{13} and Au_{32} and promotes activation of O_2.[26,27] I studied by density functional theory (DFT) calculations the structural evolution of Al_{13} as a function of the number of PVP and demonstrated for the first time that PVP can coordinate to Al_{13} while donating electronic charge. The bonding nature of PVP with Al_{13} was explained in terms of the interaction between their molecular and superatomic orbitals. Spin density analysis revealed that the Al_{13} moiety stabilized by PVP remains to be an open-shell superatom.

3.2 Computational method

In the present DFT calculations, I modeled PVP with *N*-ethyl-2-pyrrolidone (EP), which corresponds to a monomeric component of PVP. This simplification is reasonable since only a monomeric unit of each PVP may be able to interact with Al_{13}

having a highly curved potential surface. In this study, I used the B3LYP and PBE0 methods which have been used in previous studies on Al clusters.[28,29] The structures of $Al_{13}(EP)_n$ in the doublet state were optimized by the unrestricted B3LYP method for n = 0–4 with the 6-31G(d) basis set. For comparison, optimization at the PBE0/6-31G(d) level was also conducted for n = 0 and 1. Structural optimization was initiated with structures in which the O atom of EP is pointing toward or opposite to Al_{13}. The optimized structures shown in this chapter had C_1 symmetry and no imaginary frequencies. The binding energy (BE) of the EP ligand was estimated by subtracting the total electronic energy of $Al_{13}(EP)_n$ from the sum of those of $Al_{13}(EP)_{n-1}$ and EP with the zero-point energy correction. To estimate the amount of electron transfer and bonding nature of $Al_{13}(EP)_n$, the gross Mulliken charge on the Al_{13} moiety (ΔQ) was estimated. The negative value of ΔQ indicates an increase of electronic charge on Al_{13} upon ligation of EP. The calculation was conducted by the Gaussian 09 package.[30]

3.3 Results and discussion

3.3.1 Structure and stability of $Al_{13}(ligand)_1$

Figure 3.1 shows the optimized structure of Al_{13} (**0**) and Al_{13}^- (**0**$^-$) at the B3LYP/6-31G(d) level. As reported previously,[31] Al_{13}^- has an icosahedral morphology (I_h symmetry) and an electronic configuration of $(1S)^2(1P)^6(1D)^{10}(2S)^2(1F)^{14}(2P)^6$: the HOMO is not the 2P but 1F orbital because of energy splitting of 1F. In contrast, the neutral Al_{13} has a distorted structure[32] and a hole in the 1F orbital (Figure 3.2). The optimized structures of Al_{13} and Al_{13}^- at the PBE0/6-31G(d) level (Figure 3.3) were found to be similar to those in Figure 3.1. I used the B3LYP method in the following

computational surveys for the structures of $Al_{13}(EP)_n$ since the computational cost was found to be lower than that at the PBE0 method.

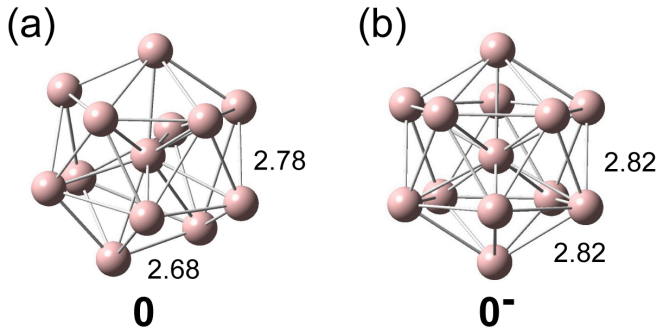

Figure 3.1. Structures of (a) Al_{13} and (b) Al_{13}^- optimized at B3LYP/6-31G(d). The numbers represent the bond lengths in Å.

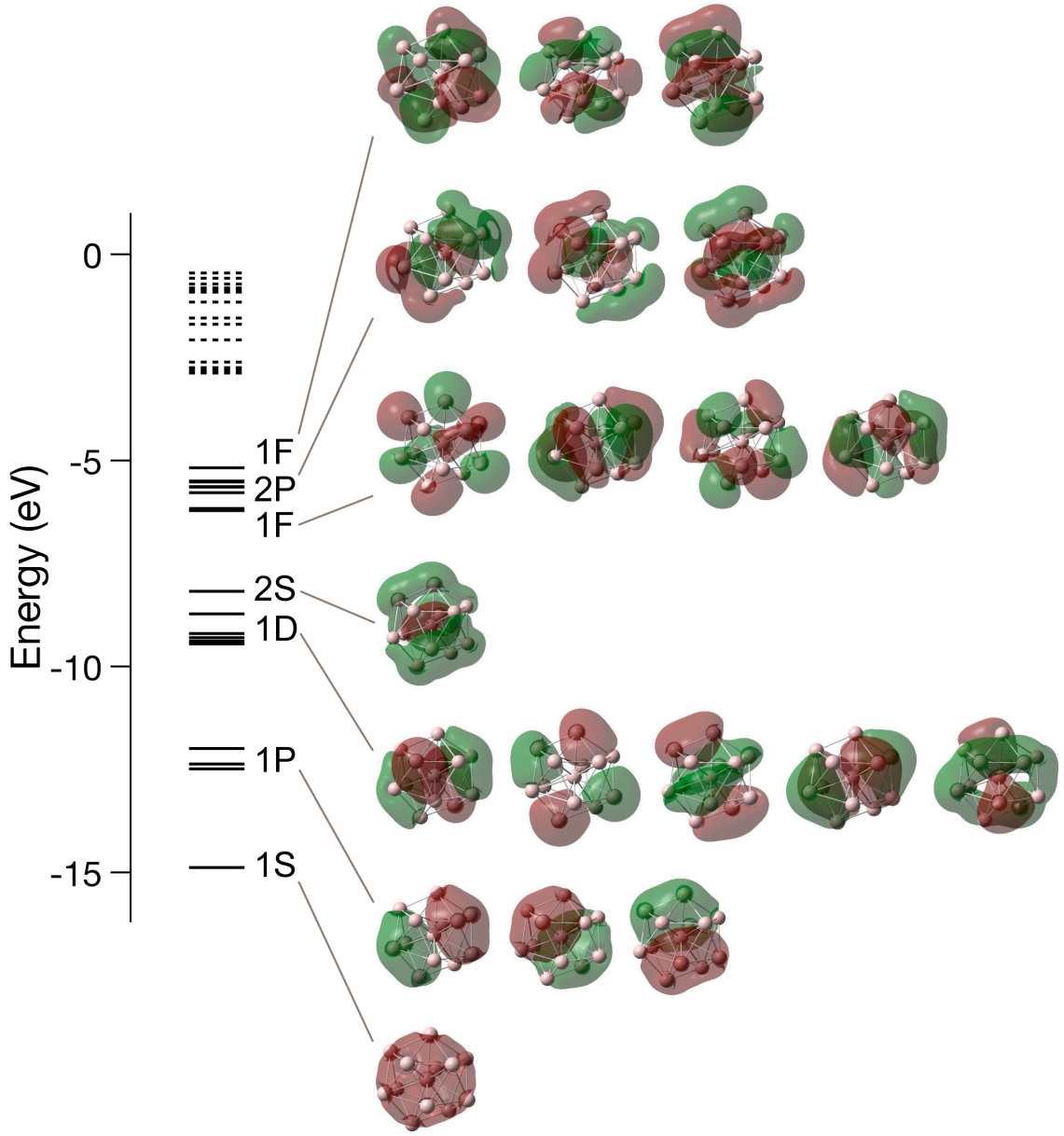

Figure 3.2. Energy diagram and superatomic orbitals of Al_{13} (**0**). The solid and dotted lines represent occupied and unoccupied orbitals, respectively.

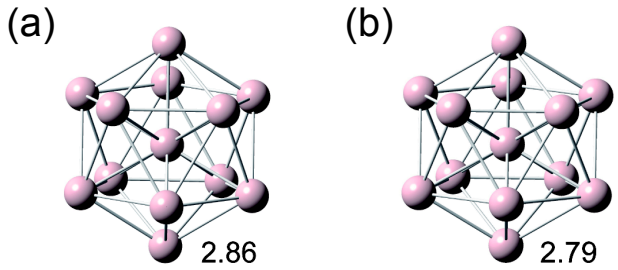

Figure 3.3. Structures of (a) Al_{13} and (b) Al_{13}^- optimized at PBE0/6-31G(d). The numbers represent the bond lengths in Å.

Figure 3.4 shows the result of extensive survey of ligand. All of ligand coordinated Al_{13} was optimized as the structure bound ligand through carbonyl oxygen with BE from 0.70 to 1.22 eV (Table 3.1). These ligands can be divided into three types. The first is the ligand with at least one nitrogen atom next to carbonyl group (Figures 3.4(a) to 3.4(e)) and ΔQ was from –0.32 to –0.36 e. The second is the ligand with carbon atom both side of carbonyl group (Figures 3.4(f) and 3.4(g)). ΔQ was still negatively with about –0.25 e. Al_{13} core coordinated by the first and second types of ligand was similar to icosahedral structure because of electron donation from ligand. On the other hand, in the third type of the ligand with hydrogen atom both side of carbonyl group (Figure 3.4(h)), ΔQ was +0.37 e and the Al_{13} core was distorted from icosahedral motif. ΔQ of the first group ligand was the most efficient donation in the three types. These ligands are likely to occur moving electrons from nitrogen to oxygen so exist resonance structure. Then the electron donation is likely to occur efficiently. But the ΔQ value was still less than –1 electron. I focused on EP that is monomer unit of PVP and searched the number of EP when the electronic shell of Al_{13} core is closed.

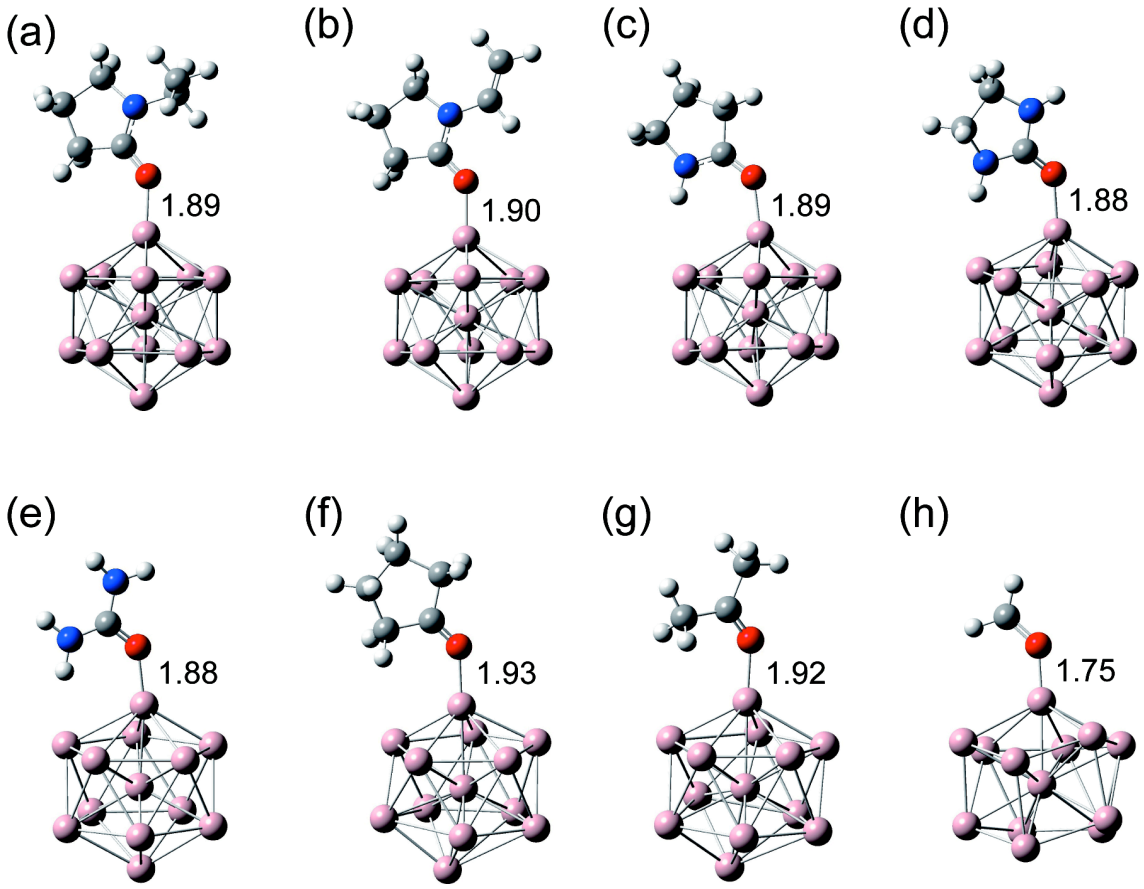

Figure 3.4. Optimized structures of Al_{13} coordinated by (a) ethylpyrrolidone, (b) vinylpyrrolidone, (c) pyrrolidone, (d) ethylene urea, (e) urea, (f) cyclopentanone, (g) acetone, and (h) formaldehyde. The numbers represent the bond lengths in Å. Key: pink = Al; red = O; gray = C; blue = N; white = H.

Table 3.1. Binding Energy and Charge Distribution of $Al_{13}(ligand)_1$.

ligand	ethyl-pyrrolidone	vinyl-pyrrolidone	pyrrolidone	ethylene urea
BE (eV)[a]	1.11	0.96	1.20	1.22
ΔQ (e)[b]	–0.36	–0.33	–0.33	–0.34
ligand	urea	cyclopentanone	acetone	formaldehyde
BE (eV)[a]	1.21	0.79	0.75	0.70
ΔQ (e)[b]	–0.32	–0.27	–0.24	+0.37

[a]Binding energy between ligand and **0**. [b]Gross Mulliken charge on the Al_{13} moiety.

3.3.2 Structure and stability of $Al_{13}(EP)_n$

Three stable structures were obtained for $Al_{13}(EP)_1$. Upon ligation of one EP to structure **0**, two stable structures **1–2** and **1–3** were obtained as shown in Figure 3.5. In both cases, the structure of Al_{13} is significantly distorted. I obtained structure **1–1** which has a symmetrical Al_{13} by using the structure of $\mathbf{0}^-$ as an initial structure. The EP molecule initially placed at the bridged or hollow site moved to a more stable atop site during the optimization. The BE and ΔQ of the three structures are listed in Table 3.2. In **1–1** and **1–2**, the EP is chemisorbed to the atop site of Al_{13} via the carbonyl O atom with the binding energy of 1.11 and 0.96 eV, respectively. The O–Al distance and C–O–Al angle of **1–1** are 1.89 Å and 136.7°, respectively. The structure of **1–1** did not change appreciably by optimization at the PBE0/6-31G(d) level (Figure 3.6). Interestingly, the gross Mulliken charge on the Al_{13} moiety in **1–1** is –0.36 e. This electron transfer is not simply due to the open electronic structure of Al_{13}, but the intrinsic electron-donating ability of the EP ligand. For example, formaldehyde is bound

to Al_{13} with the BE of 0.70 eV and takes electronic charge (ΔQ = 0.37 e) from Al_{13} (Figure 3.4(h)). As shown later, the EP ligand donates electronic charge even to Al_{13}^- having the closed electronic structure (ΔQ = –0.27 e). Okumura reported that EP can ligate and donate electronic charge to gold cluster Au_{13} (BE = 0.65 eV, ΔQ = –0.305 e).[26] On the other hand, the small BE (0.01 eV) and small electron transfer (ΔQ = –0.02 e) between EP and Al_{13} in **1–3** suggest van der Waals interaction between them. The EP is physisorbed to Al_{13} with its dipole moment (Figure 3.7) pointing toward Al_{13} so that the electrostatic interaction between the permanent dipole of EP (3.71 D) and the induced dipole on Al_{13} (polarizability = 508 au) is maximized. The results in Figure 3.5 clearly indicate that the EP ligand acts as an electron-donating ligand to Al_{13}, in sharp contrast to Cp* which acts as an electron-withdrawing ligand for Al clusters.[8,11]

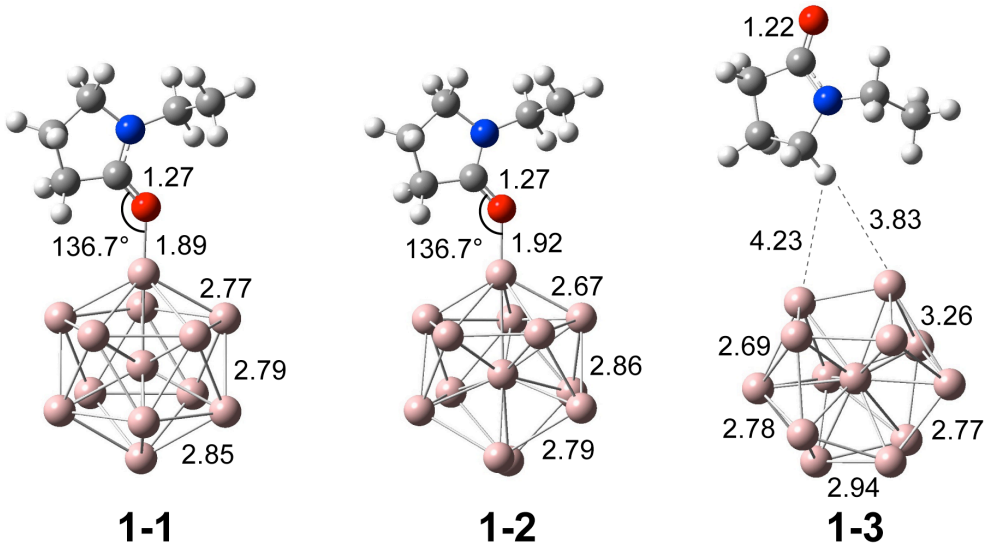

Figure 3.5. Structures of $Al_{13}(EP)_1$ optimized at B3LYP/6-31G(d). The numbers represent the bond lengths in Å. Key: pink = Al; red = O; gray = C; blue = N; white = H.

Table 3.2. Binding Energy and Charge Distribution of $Al_{13}(EP)_1$.

structure	**1–1**	**1–2**	**1–3**
BE (eV)[a]	1.11	0.96	0.01
ΔQ (e)[b]	–0.36	–0.34	–0.02

[a]Binding energy between EP and **0**. [b]Gross Mulliken charge on the Al_{13} moiety.

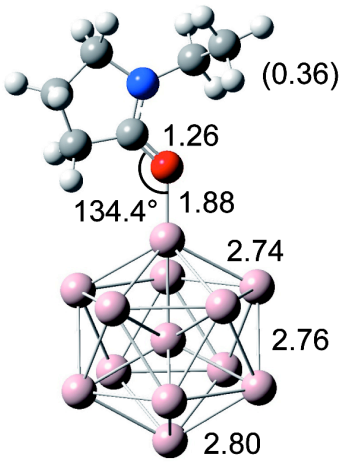

Figure 3.6. Structure of $Al_{13}(EP)_1$ optimized at PBE0/6-31G(d). The bond lengths are in the unit of Å and the numbers in parentheses represent the Mulliken charge of the EP molecules. Key: pink = Al; red = O; gray = C; blue = N; white = H.

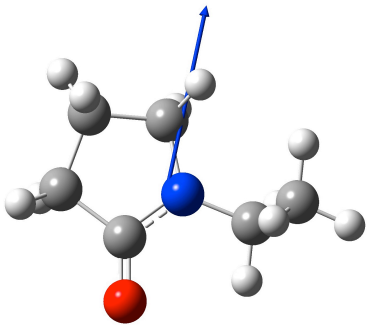

Figure 3.7. Structure of EP optimized at B3LYP/6-31G(d). The blue arrow shows the dipole moment of EP. Key: red = O; gray = C; blue = N; white = H.

Next, interaction of the second EP ligand with the most stable $Al_{13}(EP)_1$ (**1–1**) was studied. Five stable structures (Figure 3.8) were obtained for $Al_{13}(EP)_2$ after an extensive survey of initial structures. The BE and ΔQ values of each structure are summarized in Table 3.3. In structures **2–1**, **2–2**, and **2–3**, the second EP ligand is chemisorbed on the Al atoms at the ortho, meta, and para positions of the first one in **1–1**, respectively. The O–Al distances of the two EP ligands in **2–1**, **2–2**, and **2–3** are in the range of 1.90–1.97 Å, which is comparable but slightly longer than that in **1–1** (1.89 Å). The BE values of the second EP are in the range of 0.53–0.68 eV which are slightly smaller than that of the first EP in **1–1** (1.11 eV). The BEs of the second EP decrease in the order of ortho > meta > para. Regardless of the position, the second EP further donates the negative charge to the Al_{13} moiety. Increment of the gross Mulliken charge on the Al_{13} moiety (ΔΔQ) with respect to that of **1–1** (–0.36 e) was calculated to be in the range of –0.27 ~ –0.29 e.

Structures **2–4** and **2–5** in which the second EP is not chemisorbed to Al_{13} (Figure 3.8) were obtained by optimizing the initial structures in which the second EP is placed on the surface of **1–1** with the O atom pointing opposite to the Al_{13} moiety. Structures **2–4** and **2–5** were obtained when the second EP is initially placed at the ortho/meta positions and para position of the first EP, respectively. In structure **2–5**, the BE of the second EP is very small (0.04 eV), and electron transfer from the second EP is negligible (ΔΔQ = –0.01 e) as observed in **1–3**. This suggests that the second EP is physisorbed to the Al_{13} moiety via van der Waals interaction. In structure **2–4**, the second EP ligand appears to be bound to the first EP ligand with its dipole moment pointing away from the first, positively charged EP ligand (Figure 3.7). Although the BE (0.38 eV) is comparable to those for **2–1**, **2–2**, and **2–3**, the electron donation to the

Al_{13} moiety is negligible ($\Delta\Delta Q$ = –0.04 e). These features suggest that attractive interaction between the two EP ligands is mainly due to the charge-dipole interaction.

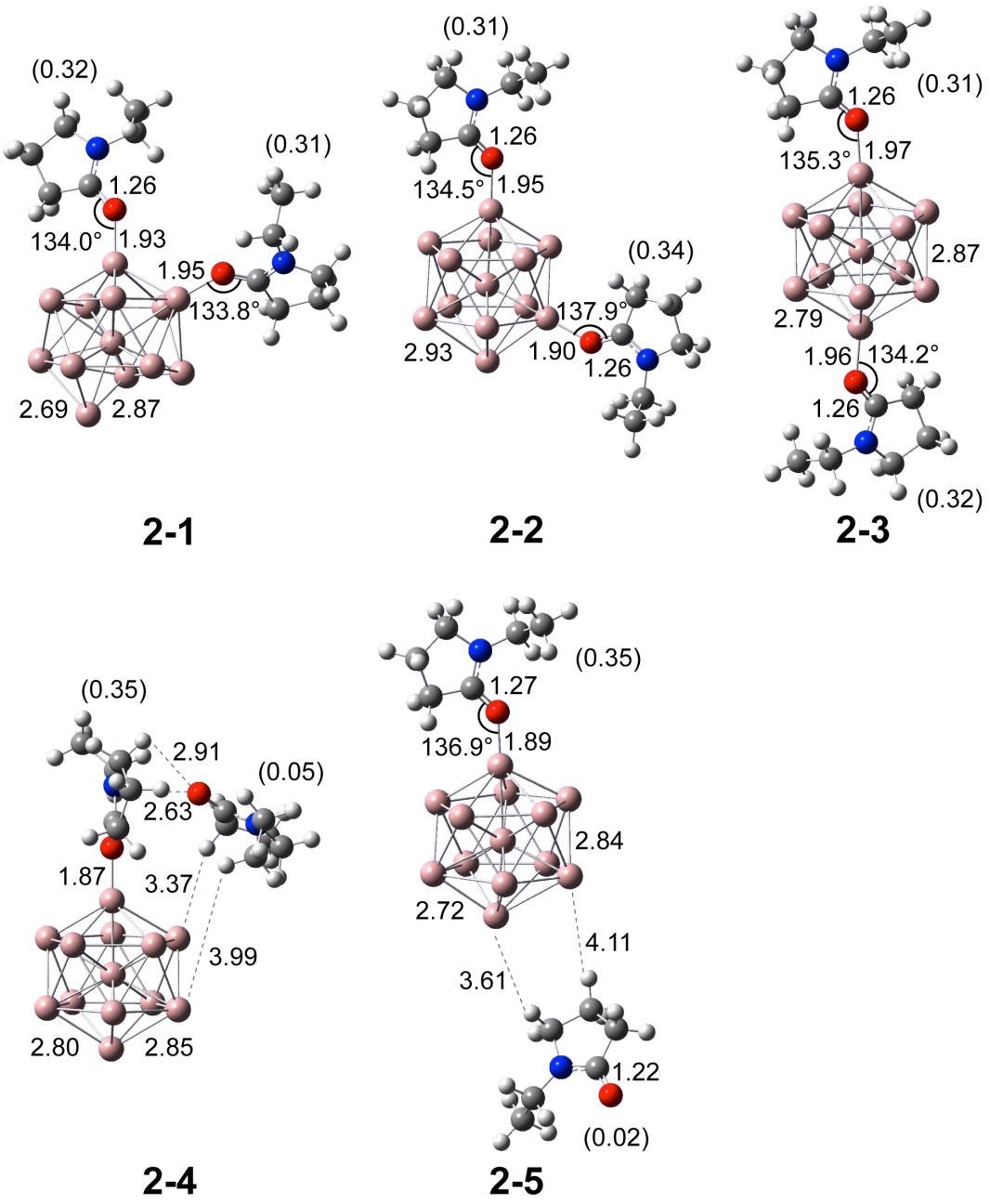

Figure 3.8. Structures of $Al_{13}(EP)_2$ optimized at B3LYP/6-31G(d). The bond lengths are in the unit of Å, and the numbers in parentheses represent the Mulliken charge of the EP ligands. Key: pink = Al; red = O; gray = C; blue = N; white = H.

Table 3.3. Binding Energy and Charge Distribution of $Al_{13}(EP)_2$.

structure	**2–1**	**2–2**	**2–3**	**2–4**	**2–5**
BE (eV)[a]	0.68	0.65	0.53	0.38	0.04
ΔQ (e)[b]	–0.63	–0.65	–0.63	–0.40	–0.37
ΔΔQ (e)[c]	–0.27	–0.29	–0.27	–0.04	–0.01

[a]Binding energy of EP with respect to **1–1**. [b]Gross Mulliken charge on the Al_{13} moiety. [c]Increment of the gross Mulliken charge on the Al_{13} moiety with respect to that of **1–1** (–0.36 e).

Figures 3.5 and 3.8 indicate that chemisorption is energetically the most preferable interaction for the first and second EP ligands. This trend further continued to the third EP ligand in $Al_{13}(EP)_3$. Figure 3.9 shows five optimized structures **3–1** to **3–5** in which the third EP ligands are chemisorbed to different sites of two precursors $Al_{13}(EP)_2$ (**2–1** and **2–2**). Table 3.4 shows the BE and ΔQ of the five structures. Regardless of the coordination sites, the O–Al distances of the three EP ligands are in the range of 1.91–2.00 Å. The BEs of the third EP in **3–1** to **3–5** are in the range of 0.33–0.50 eV with respect to the corresponding precursors (**2–1** and **2–2**), which are slightly smaller than those of the first and second EP ligands. The third EP ligand further increased the electronic charge of the Al_{13} moiety by $\Delta\Delta Q = -0.25 \sim -0.29$ e. As a result, the total charge accumulated by the chemisorption of the three EP ligands amounts to almost –1 e.

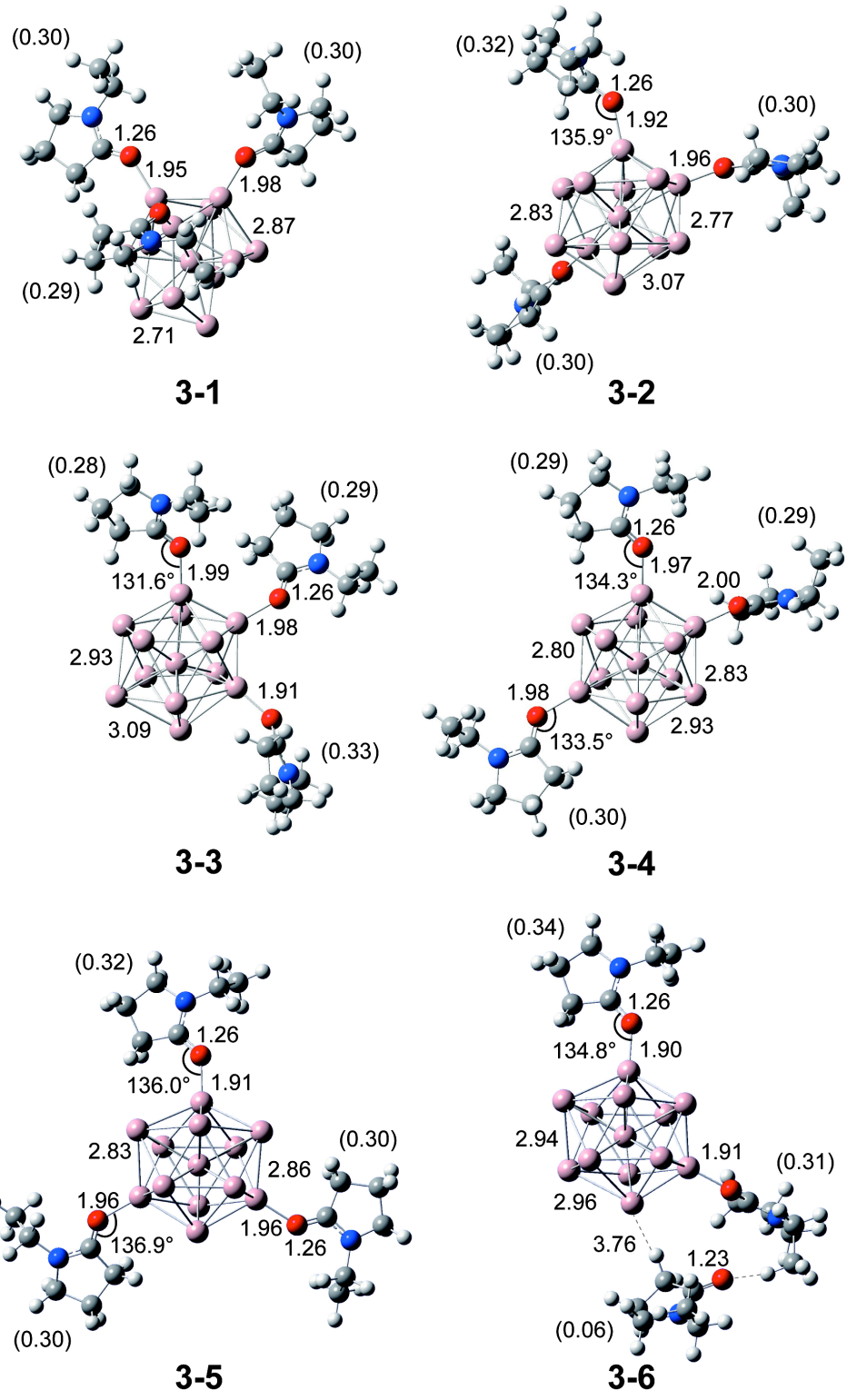

Figure 3.9. Structures of $Al_{13}(EP)_3$ optimized at B3LYP/6-31G(d). The bond lengths are in the unit of Å, and the numbers in parentheses represent the Mulliken charge of the EP ligands. Key: pink = Al; red = O; gray = C; blue = N; white = H.

Table 3.4. Binding Energy and Charge Distribution of $Al_{13}(EP)_3$.

structure	**3–1**	**3–2**	**3–3**	**3–4**	**3–5**	**3–6**
precursor		**2–1**			**2–2**	
ΔE (eV)[a]	0.01	0.01	0.09	0.13	0.00	0.09
BE (eV)[b]	0.45	0.45	0.37	0.33	0.50	0.41
ΔQ (e)[c]	–0.89	–0.92	–0.90	–0.88	–0.92	–0.71
ΔΔQ (e)[d]	–0.26	–0.29	–0.27	–0.25	–0.27	–0.06

[a]Relative stability of $Al_{13}(EP)_3$. [b]Binding energy of EP with respect to precursor. [c]Gross Mulliken charge on the Al_{13} moiety. [d]Increment of the gross Mulliken charge on the Al_{13} moiety with respect to that of precursor.

I also obtained structure **3–6** in which the third EP is bound to one of the EP ligands of **2–2** via charge-dipole interaction as can be seen in **2–4**. Although the BE (0.41 eV) is comparable to those for chemisorption (0.33–0.50 eV) in the other five structures, the electron transfer to Al_{13} is negligibly small (ΔΔQ = –0.06 e).

It is interesting to see how the fourth EP ligand interacts with $Al_{13}(EP)_3$ after the Al_{13} moiety accepts ~1 e Mulliken charge from the three EP ligands. Among the ten possible combinations to coordinate four EP ligands on Al_{13} (Figure 3.10), I focused only on the structures obtained by binding the fourth EP to the most stable structure of $Al_{13}(EP)_3$ (**3–5**). As a result, four optimized structures were obtained as shown in Figure 3.11. The BE and ΔQ of the four structures are listed in Table 3.5. In **4–2**, **4–3**, and **4–4**, the fourth EP ligand further donates electronic charges (ΔΔQ = –0.18 ~ –0.24 e) to Al_{13} via chemisorption (BEs = 0.14–0.35 eV). More importantly, the most stable structure

was **4–1** in which the fourth EP ligand is not chemisorbed on Al_{13} but is bound to one of the chemisorbed EP ligands with the BE of 0.38 eV as in the case of **2–4** and **3–6**. As expected, the electronic charge is not transferred to Al_{13} from the fourth EP.

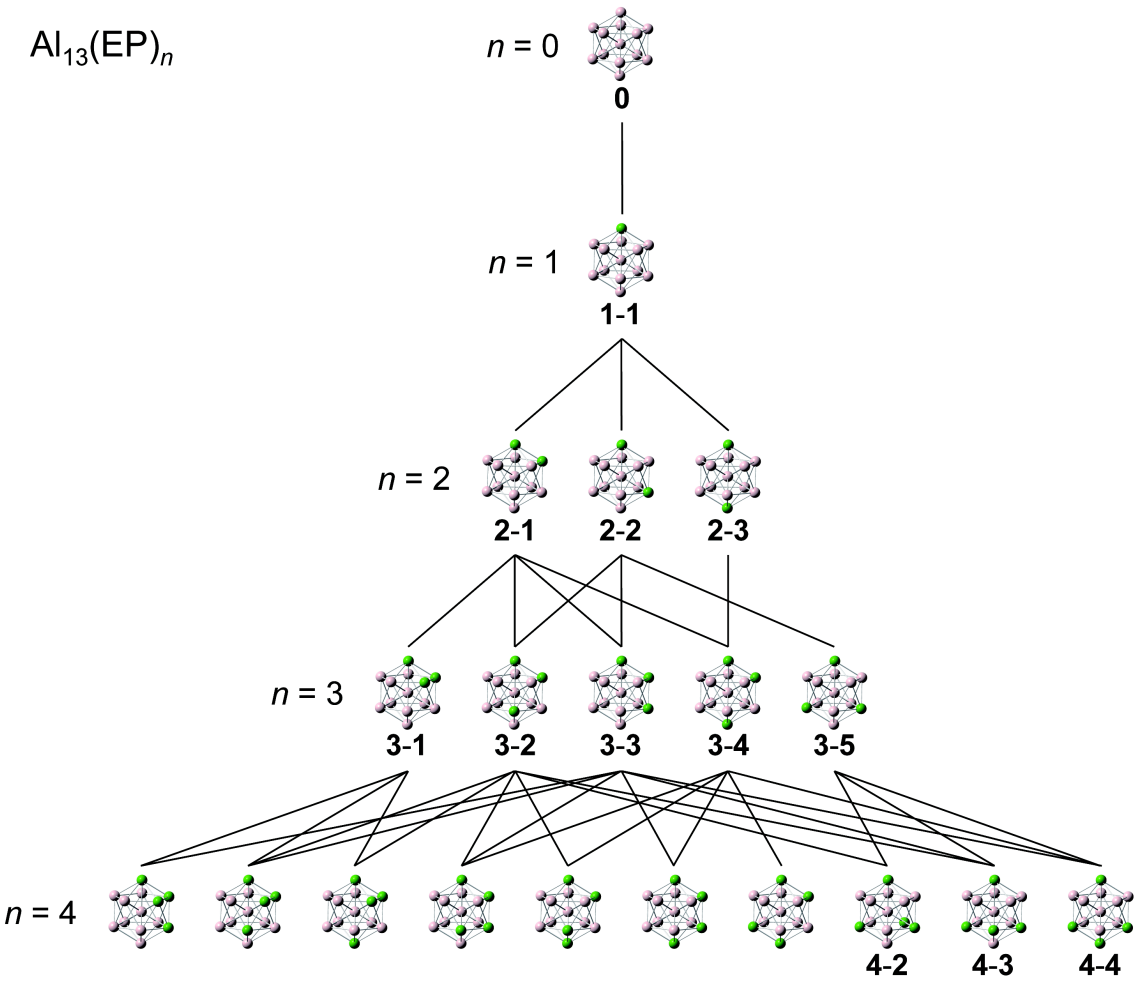

Figure 3.10. Tree diagram of possible coordination sites of $Al_{13}(EP)_n$. Green balls indicate the atom bound to EP.

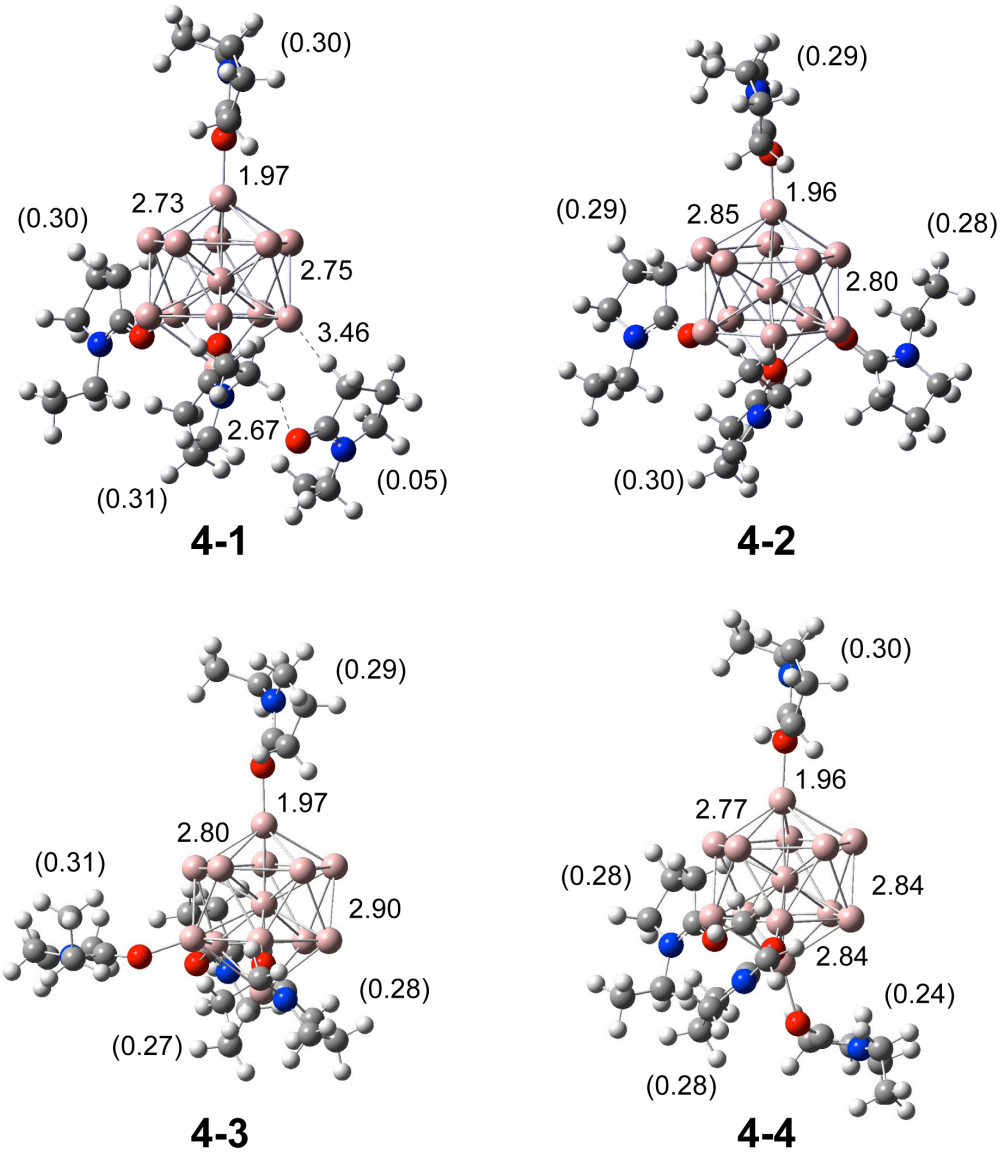

Figure 3.11. Structures of $Al_{13}(EP)_4$ optimized at B3LYP/6-31G(d). The bond lengths are in the unit of Å, and the numbers in parentheses represent the Mulliken charge of the EP ligands. Key: pink = Al; red = O; gray = C; blue = N; white = H.

Table 3.5. Binding Energy and Charge Distribution of $Al_{13}(EP)_4$.

structure	**4–1**	**4–2**	**4–3**	**4–4**
BE (eV)[a]	0.38	0.35	0.24	0.14
ΔQ (e)[b]	–0.96	–1.16	–1.15	–1.10
ΔΔQ (e)[c]	–0.04	–0.24	–0.23	–0.18

[a]Binding energy of EP with respect to **3–5**. [b]Gross Mulliken charge on the Al_{13} moiety. [c]Increment of the gross Mulliken charge on the Al_{13} moiety with respect to that of **3–5** (–0.92 e).

3.3.3 Switchover of the bonding scheme in $Al_{13}(EP)_n$

As demonstrated above, the preferential bonding scheme of EP ligands changes from chemisorption to Al_{13} to bonding to another ligand via electrostatic interaction at the fourth EP. Figure 3.12 shows the energy diagram of stepwise ligation of $Al_{13}(EP)_n$. Black lines indicate the energy levels of $Al_{13}(EP)_n$ with all the EP ligands chemisorbed to Al_{13}, while green lines represent the energy levels of $Al_{13}(EP)_n$ with one of the EP ligands weakly bound to another chemisorbed EP ligand. The incremental chemisorption energy of $Al_{13}(EP)_n$ was calculated to be 1.1, 0.7, 0.5, and 0.35 eV for n = 1–4, respectively, from the energy difference between the most stable isomers (**0**, **1–1**, **2–1**, **3–5**, and **4–2**). In contrast, the stepwise binding energy of EP toward the already chemisorbed EP in $Al_{13}(EP)_n$ was calculated to be 0.38, 0.41, and 0.38 eV for n = 2–4, respectively, from the energy difference between the most stable isomers (**1–1**, **2–4**, **3–6**, and **4–1**). The chemisorption energy monotonically decreased with n probably due to the gradual accumulation of the negative charge to the Al_{13} moiety, while the electrostatic interaction is nearly constant regardless of n. This trend in the binding

energies is the major reason for this switchover of the bonding scheme. The switchover behavior observed here suggests that the maximum number of PVP that can be chemisorbed on metal clusters is determined not only by the steric repulsion between adjacent PVP but also by the electronic charge accumulated on the clusters.

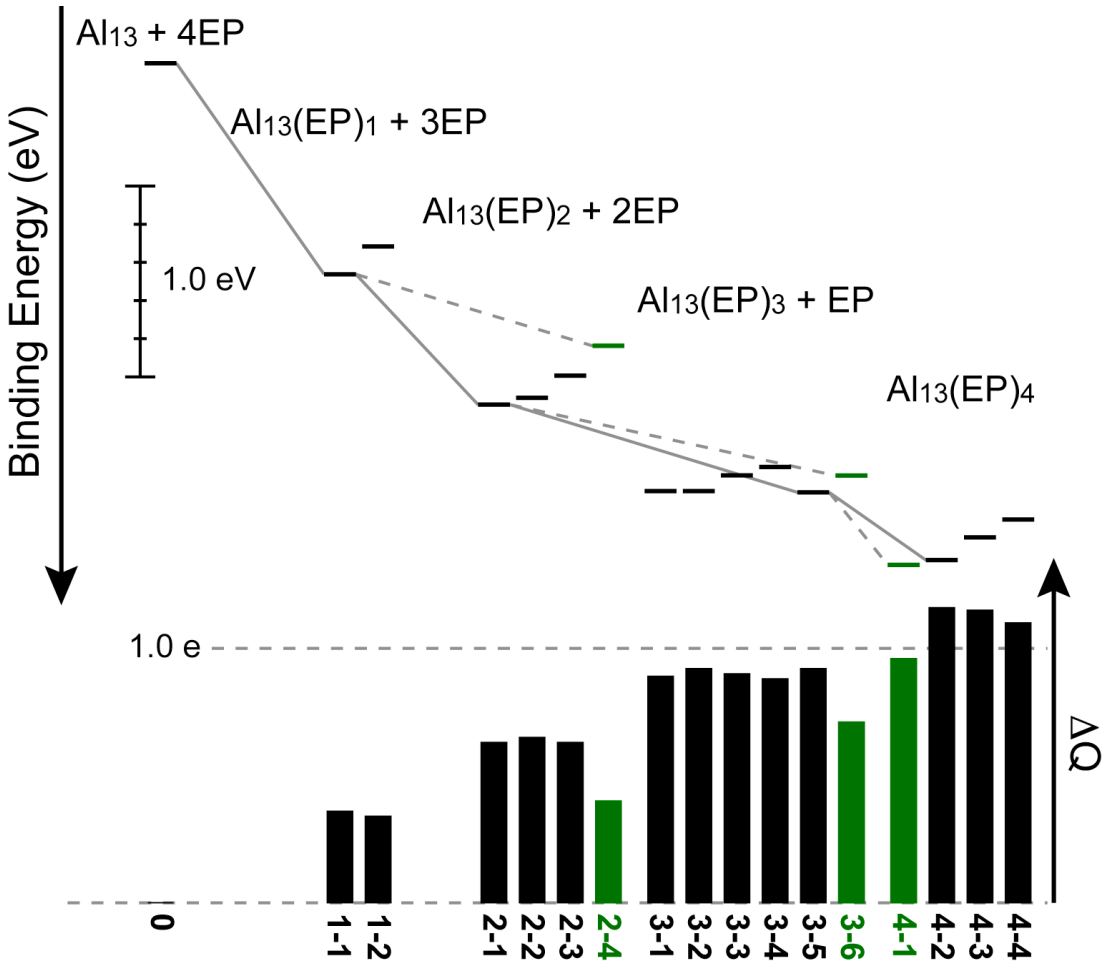

Figure 3.12. Energy diagram of stepwise ligation of $Al_{13}(EP)_n$. The horizontal lines in the upper panel and solid bars in the lower panel represent BE and ΔQ with respect to **0**, respectively. Black color indicates that all the EP ligands are chemisorbed to Al_{13}, while green color indicates that one of the EP ligands is weakly bound to another chemisorbed EP ligand.

3.3.4 Bonding interaction between Al_{13} and EP

In Figure 3.12, the gross Mulliken charges of $Al_{13}(EP)_n$ are shown by vertical bars. It appears that the switchover of the bonding scheme occurs when the Mulliken charge reaches –1 e at $Al_{13}(EP)_3$, suggesting that this phenomenon is associated with closure of the electronic shell of the Al_{13} superatom in $Al_{13}(EP)_3$ (**3–5**). The electronic shell closure of the Al_{13} moiety in $Al_{13}(EP)_3$ is also suggested by the fact that the chemisorption energies of the fourth EP to $Al_{13}(EP)_3$ (**3–5**) (0.14–0.35 eV, Table 3.5) are comparable to that of EP to the electronically closed superatom Al_{13}^- (0.23 eV, Table 3.6). In order to test this hypothesis, I examined the bonding interaction between EP and Al_{13}. I first compared the shapes of SOMOs of Al_{13} and $Al_{13}(EP)_1$ (**1–1**) to see whether SOMO of Al_{13} and HOMO or LUMO of EP are involved in the bonding. As shown in Figures 3.13(a) and 3.13(b), the SOMOs of $Al_{13}(EP)_1$ and Al_{13} look similar in shape, indicating that interaction of frontier orbitals of Al_{13} and EP is small and not the origin of the bonding stabilization. I searched for MOs of $Al_{13}(EP)_1$ in which the electrons are distributed over the frameworks of Al_{13} and EP. Such analysis revealed that three sets of bonding and antibonding MOs are constructed from occupied 1S, 1P, and 1D orbitals of Al_{13} and occupied MOs of EP (Figure 3.14). Although both the bonding and antibonding MOs were fully occupied, the energy gained by occupation of bonding MOs was larger than the destabilization energy by occupation of antibonding MOs. Especially, the stabilization energies derived from 1S and 1D orbitals were larger than that from 1P. This is due to efficient overlap of the p orbital of the carbonyl O atom with the 1S or 1D superatomic orbital of Al_{13} (Figures 3.13(c) and 3.13(d)). Namely, electronic charge is formally transferred from PVP to Al_{13} through polarized Al–O bonding between EP and Al_{13} superatom.

Table 3.6. Optimized Structure, Binding Energy, and Charge Distribution of $Al_{13}(EP)_1^-$ at the Level of B3LYP/6-31G(d). The bond lengths are in the unit of Å and the numbers. Key: pink = Al; red = O; gray = C; blue = N; white = H.

	1	**2**
optimized structure	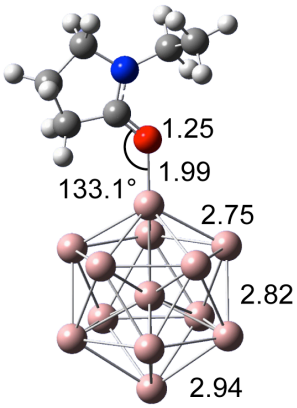	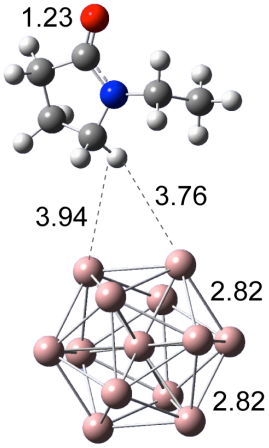
BE (eV)[a]	0.23	0.15
ΔQ (e)[b]	–0.27	–0.01

[a]Binding energy between EP and Al_{13}^-. [b]Gross Mulliken charge on the Al_{13} moiety.

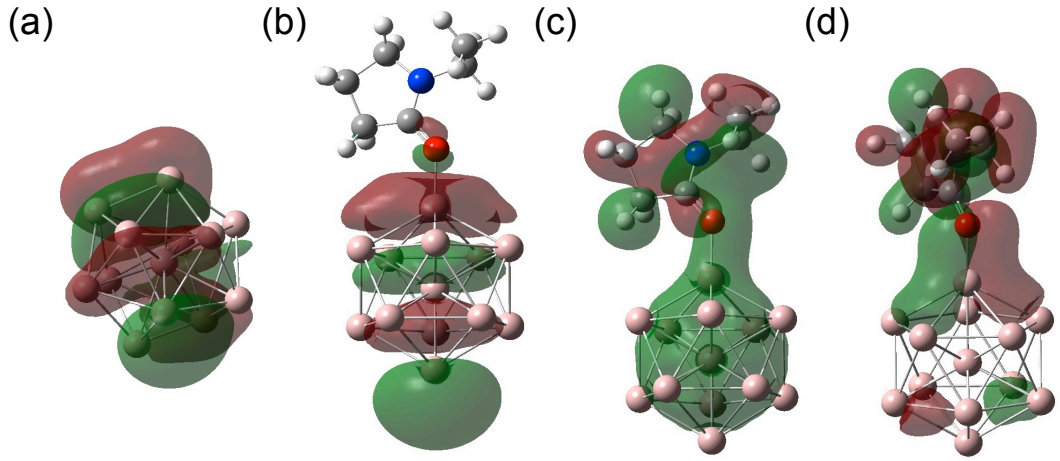

Figure 3.13. Shapes of SOMO of (a) Al_{13} (**0**) and (b) $Al_{13}(EP)_1$ (**1–1**) and bonding MOs of $Al_{13}(EP)_1$ (**1–1**) constructed by (c) 1S and (d) 1D superatomic orbitals of Al_{13}.

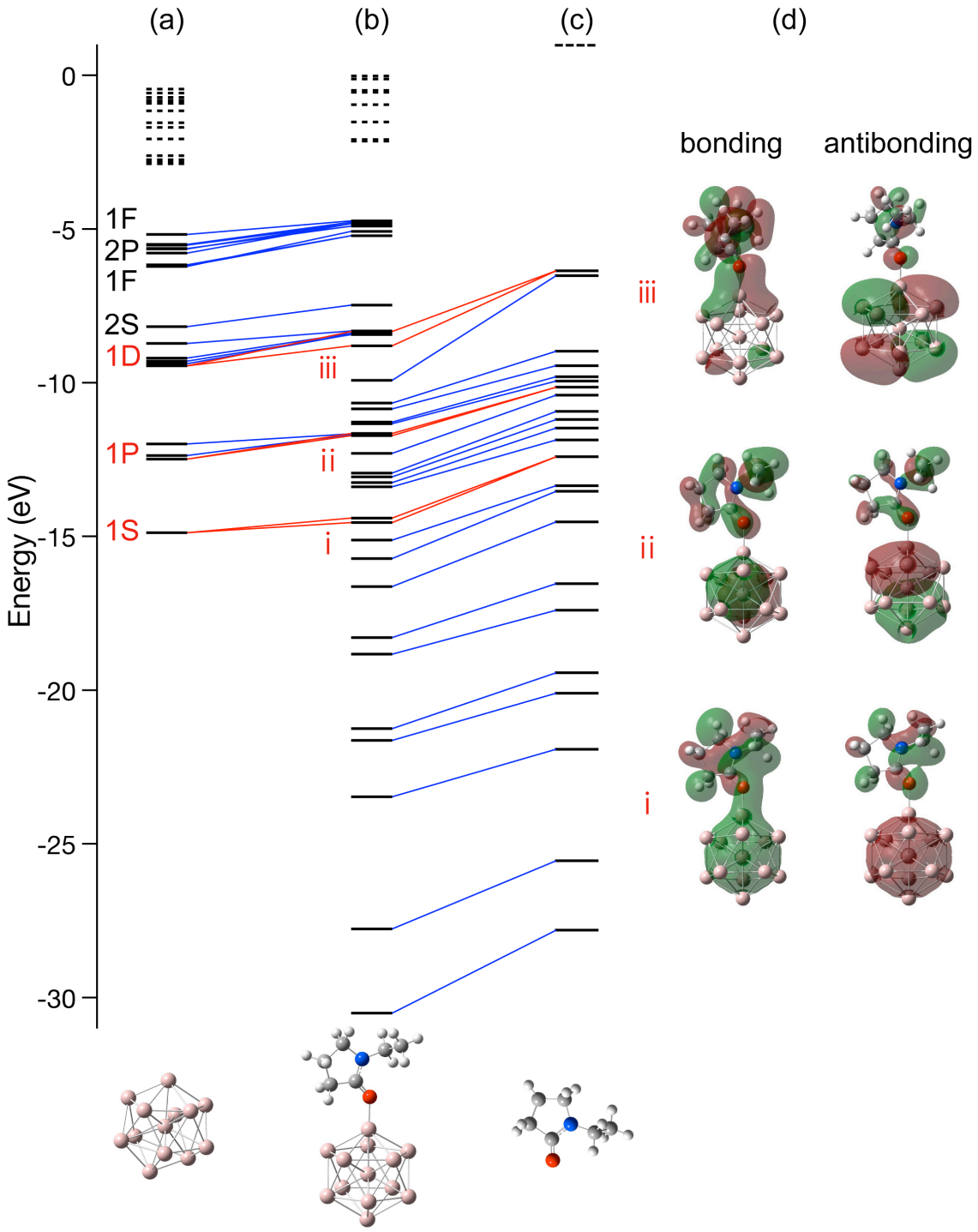

Figure 3.14. Energy diagram of (a) Al_{13} (**0**), (b) $Al_{13}(EP)_1$ (**1–1**), and (c) EP. The solid and dotted lines represent occupied and unoccupied orbitals, respectively. (d) Bonding and antibonding MOs of $Al_{13}(EP)_1$ constructed by 1S, 1P, and 1D superatomic orbitals of Al_{13}.

I further examined spin density of $Al_{13}(EP)_3$ (**3–5**). The calculated spin density isosurface (Figure 3.15) is very similar to shapes of SOMOs of $Al_{13}(EP)_3$ and $Al_{13}(EP)_1$ (**1–1**) (Figure 3.13(b)). This result indicates that the superatomic orbital 1F of Al_{13} remains singly occupied even after chemisorption of three EP ligands. Namely, the electronic shell of Al_{13} is not closed although the EP ligands donate electronic charge. The above analysis implies that energy matching and efficient overlap between the relevant MO of the ligand and 1F superatomic orbital are required in order to fill up the superatomic orbitals of Al_{13} by ligation.

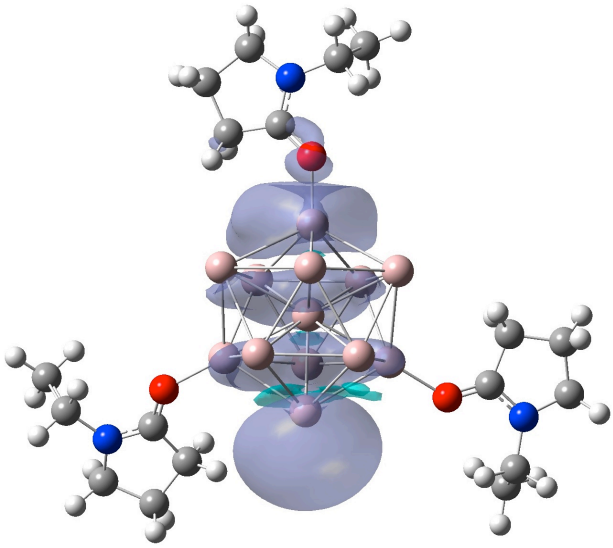

Figure 3.15. Spin density isosurface of $Al_{13}(EP)_3$ (**3–5**).

3.4 Conclusion

I studied the structures of $Al_{13}(EP)_n$ (n = 0–4) by DFT calculations to elucidate the bonding nature between PVP and Al_{13} and to explore the possibility that Al_{13} can be stabilized by closure of the electronic shells via ligation of PVP. The

optimized structure of $Al_{13}(EP)_1$ indicated that the EP ligand is chemisorbed to the atop site of Al_{13} via the carbonyl O atom, while donating –0.36 e to the Al_{13} moiety. The stabilization is mainly due to bonding interaction between molecular orbitals of EP and the 1S or 1D superatomic orbital of Al_{13}. The chemisorption to the Al_{13} moiety is energetically preferred up to three EP ligands, and the total charge accumulated in Al_{13} reaches nearly –1 e in $Al_{13}(EP)_3$. The fourth EP ligand, however, prefers to be bound to one of the chemisorbed EP ligands via electrostatic interaction rather than to be chemisorbed on Al_{13}. The switchover of the bonding scheme of EP at $Al_{13}(EP)_4$ suggests that this phenomenon is associated with closure of the electronic shell of the Al_{13} moiety in $Al_{13}(EP)_3$. However, spin density analysis revealed that the superatomic orbital 1F of Al_{13} remains singly occupied even after chemisorption of three EP ligands. In conclusion, chemisorption of EP ligands to Al_{13} does not lead to the filling of the superatomic orbital 1F, but formally donates electronic charge through polarized Al–O bonding.

References

1. Armstrong, R. W.; Baschung, B.; Booth, D. W.; Samirant, M. *Nano Lett.* **2003**, *3*, 253.
2. Ghanta, S. R.; Muralidharan, K. *Nanoscale* **2010**, *2*, 976.
3. Lewis, W. K.; Harruff, B. A.; Gord, J. R.; Rosenberger, A. T.; Sexton, T. M.; Guliants, E. A.; Bunker, C. E. *J. Phys. Chem. C* **2011**, *115*, 70.
4. Wu, B.; Liu, X.; Oo, T. Z.; Xing, G.; Mathews, N.; Sum, T. C. *Plasmonics* **2012**, *7*, 677.
5. Chong, X.; Jiang, N.; Zhang, Z.; Roy, S.; Gord, J. R. *J. Nanopart. Res*. **2013**, *15*, 1678.
6. Bunker, C. E.; Smith, M. J.; Fernando, K. A. S.; Harruff, B. A.; Lewis, W. K.; Gord, J. R.; Guliants, E. A.; Phelps, D. K. *ACS Appl. Mater. Interfaces* **2010**, *2*, 11.
7. Viau, G.; Collière, V.; Lacroix, L. M.; Shafeev, G. A. *Chem. Phys. Lett*. **2011**, *501*, 419.
8. Schnöckel, H. *Chem. Rev.* **2010**, *110*, 4125.
9. Walter, M.; Akola, J.; Lopez-Acevedo, O.; Jadzinsky, P. D.; Calero, G.; Ackerson, C. J.; Whetten, R. L.; Grönbeck, H.; Häkkinen, H. *Proc. Natl. Acad. Sci. U. S. A*. **2008**, *105*, 9157.
10. Li, X.; Wu, H.; Wang, X. B.; Wang, L. S. *Phys. Rev. Lett.* **1998**, *81*, 1909.
11. Clayborne, P. A.; Lopez-Acevedo, O.; Whetten, R. L.; Grönbeck, H.; Häkkinen, H. *Eur. J. Inorg. Chem.* **2011**, 2649.
12. Castleman, A. W.; Khanna, S. N. *J. Phys. Chem. C* **2009**, *113*, 2664.
13. de Heer, W. A. *Rev. Mod. Phys*. **1993**, *65*, 611.
14. Alnemrat, S.; Hooper, J. P. *J. Chem. Phys*. **2014**, *140*, 104313.
15. Leuchtner, R. E.; Harms, A. C.; Castleman, A. W. *J. Chem. Phys.* **1991**, *94*, 1093.
16. Reber, A. C.; Khanna, S. N.; Roach, P. J.; Woodward, W. H.; Castleman, A. W. *J. Phys. Chem. A* **2010**, *114*, 6071.
17. Luo, Z.; Smith, J. C.; Woodward, W. H.; Castleman, A. W. *J. Phys. Chem. Lett.* **2012**, *3*, 3818.
18. Neumaier, M.; Olzmann, M.; Kiran, B.; Bowen, K. H.; Eichhorn, B.; Stokes, S. T.; Buonaugurio, A.; Burgert, R.; Schnöckel, H. *J. Am. Chem. Soc.* **2014**, *136*, 3607.
19. Nakajima, A.; Hoshino, K.; Naganuma, T.; Sone, Y.; Kaya, K. *J. Chem. Phys.* **1991**, *95*, 7061.
20. Ko, Y. J.; Shakya, A.; Wang, H.; Grubisic, A.; Zheng, W.; Götz, M.; Ganteför, G.; Bowen, K. H.; Jena, P.; Kiran, B. *J. Chem. Phys.* **2010**, *133*, 124308.
21. Qiu, L.; Liu, F.; Zhao, L.; Yang, W.; Yao, J. *Langmuir* **2006**, *22*, 4480.
22. Hossain, M. J.; Tsunoyama, H.; Yamauchi, M.; Ichikuni, N.; Tsukuda, T. *Catal. Today* **2012**, *183*, 101.
23. Tongsakul, D.; Nishimura, S.; Ebitani, K. *J. Phys. Chem. C* **2014**, *118*, 11723.

24. Jiang, P.; Zhou, J. J.; Li, R.; Wang, Z. L.; Xie, S. S. *Nanotechnology* **2006**, *17*, 3533.
25. Tsunoyama, H.; Ichikuni, N.; Sakurai, H.; Tsukuda, T. *J. Am. Chem. Soc*. **2009**, *131*, 7086.
26. Okumura, M.; Kitagawa, Y.; Kawakami, T.; Haruta, M. *Chem. Phys. Lett*. **2008**, *459*, 133.
27. Yu, S.; Zeng, Q.; Lou, Z.; Yang, M.; Wu, D. *Phys. Chem. Chem. Phys.* **2013**, *15*, 9742.
28. Smith, Q. A.; Gordon, M. S. *J. Phys. Chem. A*, **2011**, *115*, 899.
29. Aguado, A.; López, J. M. *J. Chem. Phys*. **2009**, *130*, 064704.
30. Frisch, M. J.; Trucks, G. W.; Schlegel, H. B.; Scuseria, G. E.; Robb, M. A.; Cheeseman, J. R.; Scalmani, G.; Barone, V.; Mennucci, B.; Petersson, G. A.; Nakatsuji, H.; Caricato, M.; Li, X.; Hratchian, H. P.; Izmaylov, A. F.; Bloino, J.; Zheng, G.; Sonnenberg, J. L.; Hada, M.; Ehara, M.; Toyota, K.; Fukuda, R.; Hasegawa, J.; Ishida, M.; Nakajima, T.; Honda, Y.; Kitao, O.; Nakai, H.; Vreven, T.; Montgomery, J. A., Jr.; Peralta, J. E.; Ogliaro, F.; Bearpark, M.; Heyd, J. J.; Brothers, E.; Kudin, K. N.; Staroverov, V. N.; Keith, T.; Kobayashi, R.; Normand, J.; Raghavachari, K.; Rendell, A.; Burant, J. C.; Iyengar, S. S.; Tomasi, J.; Cossi, M.; Rega, N.; Millam, J. M.; Klene, M.; Knox, J. E.; Cross, J. B.; Bakken, V.; Adamo, C.; Jaramillo, J.; Gomperts, R.; Stratmann, R. E.; Yazyev, O.; Austin, A. J.; Cammi, R.; Pomelli, C.; Ochterski, J. W.; Martin, R. L.; Morokuma, K.; Zakrzewski, V. G.; Voth, G. A.; Salvador, P.; Dannenberg, J. J.; Dapprich, S.; Daniels, A. D.; Farkas, O.; Foresman, J. B.; Ortiz, J. V.; Cioslowski, J.; Fox, D. J. *Gaussian 09*, *Revision C.01*, Gaussian, Inc., Wallingford CT, 2010.
31. Han, Y. K.; Jung, J. *J. Am. Chem. Soc.* **2008**, *130*, 2.
32. Zhao, J. Y.; Zhao, F. Q.; Gao, H. X.; Ju, X. H. *J. Mol. Model.* **2013**, *19*, 1789.

Chapter 4.

Concluding remarks

To obtain a hint toward synthesis of superatomic Al_{13} based materials, I investigated two themes about Al_{13} contains clusters. In chapter 2, chemical reactions of Al_n^- under high-pressure O_2 were investigated to gain insights into the stability of Al_{13}^- under atmospheric conditions. In chapter 3, interaction between open-shell Al_{13} with electron donating ligand with carbonyl group was studied by density functional theory (DFT) calculations to test the hypothesis that the electronic shell of Al_{13} can be closed by electron donation from ligands. In the followings, I summarize about each theme and describe about future prospects.

4.1 Production of new aluminum oxide clusters having Al_{13} core

Al_n^- were generated by laser vaporization and were allowed to pass through a cell in which O_2 was filled. Compositions of the reaction products were determined by time-of-flight mass spectrometer. The reaction of Al_n^- and O_2 under a high-pressure condition yielded the previously unknown aluminum oxides $Al_{14}O^-$ and $Al_{15}O_2^-$. Electronic and geometric structures of the new magic clusters, $Al_{14}O^-$ and $Al_{15}O_2^-$, were studied by magnetic bottle-type photoelectron spectrometer and DFT calculations. The VDEs of $Al_{14}O^-$ and $Al_{15}O_2^-$ were determined to be 3.84 ± 0.02 and 3.88 ± 0.02 eV, respectively. DFT calculations at the B3LYP/6-31G(d) level predicted that the most stable isomeric structures $Al_{14}O^-$ and $Al_{15}O_2^-$ are composed of icosahedral Al_{13} and one or two OAl unit(s), respectively. The VDE values of these structures calculated (3.27 and 3.28 eV, respectively) reproduced the experimental values. It is known that reaction of Al_n^- ($n \geq 8$) with O_2 proceeds by releasing a highly stable fragment Al_2O. In the framework of this reaction path, $Al_{14}O^-$ and $Al_{15}O_2^-$ correspond to intermediates of oxidative etching reactions of Al_{16}^- and Al_{15}^-, respectively. According to DFT

calculations, removal of an extra Al_2O from $Al_{14}O^-$ and $Al_{15}O_2^-$ is endothermic by 1.78 and 1.92 eV, respectively. The preferential formation of $Al_{14}O^-$ and $Al_{15}O_2^-$ was due to their high stability associated with the Al_{13} moiety and the efficient dissipation of reaction exothermicity by collisional cooling.

4.2 Stabilization of Al_{13} by electron donating ligand

From the DFT calculations of structures of Al_{13} coordinated by ligand with carbonyl group, it was found that ligands with nitrogen atom or two carbon atoms next to carbonyl group could donate electron to Al_{13}. Then the structures of $Al_{13}(EP)_n$ (n = 0–4) were extensively investigated to test the possibility that Al_{13} can be stabilized by closure of the electronic shells via ligation of PVP. The optimized structure of $Al_{13}(EP)_1$ indicated that the EP ligand is chemisorbed to the atop site of Al_{13} via the carbonyl O atom, while donating –0.36 e to the Al_{13} moiety. The chemisorption to the Al_{13} moiety is energetically preferred up to three EP ligands and the total charge accumulated in Al_{13} reaches nearly –1 e in $Al_{13}(EP)_3$. The fourth EP ligand, however, prefers to be bound to one of the chemisorbed EP ligands via electrostatic interaction rather than to be chemisorbed on Al_{13}. The switchover of the bonding scheme of EP at $Al_{13}(EP)_4$ suggests that this phenomenon is associated with closure of the electronic shell of the Al_{13} moiety in $Al_{13}(EP)_3$. However, spin density analysis revealed that the superatomic orbital 1F of Al_{13} remains singly occupied even after chemisorption of three EP ligands. In conclusion, chemisorption of EP ligands to Al_{13} does not lead to the filling of the superatomic orbital 1F, but formally donates electronic charge through polarized Al–O bonding.

4.3 Future prospects on Al_{13}-based materials

From the reaction under high pressure O_2, it was found that Al_{13}^-, $Al_{14}O^-$, and $Al_{15}O_2^-$ showed high mass abundance. This result suggests that the icosahedral containing clusters prohibit further oxidative etching by O_2. These cluster anions are expected to exist in the air without decomposition when the negative charges are kept on them. In addition, it is also expected that combustion of large aluminum clusters will terminate when these Al_{13}-based clusters are obtained. Therefore, there is a possibility of size-focused synthesis of Al_{13}-based materials by etching reaction in the air. For example, widely size distributed aluminum clusters that are generated in gas phase may be size-focused to Al_{13} containing clusters by exposing to the air.

DFT calculation about interaction between Al_{13} and ligand with carbonyl group revealed that Al_{13} could be stabilized by chemisorption of the ligands but its electronic shell was not closed. The reason seems that the overlap between frontier orbitals of Al_{13} and ligand is not efficiently. Then there is a possibility that other ligand that its frontier orbitals can strongly interact with those of Al_{13} may make the electronic shell of Al_{13} closed.

Appendix.

List of publication and presentation

Publications related to the thesis

1. "Structural Characterization of Unprecedented $Al_{14}O^-$ and $Al_{15}O_2^-$: Photoelectron Spectroscopy and Density Functional Calculations", Tomomi Watanabe and Tatsuya Tsukuda, *J. Phys. Chem. C*, **2013**, *117*, 6664-6668.
2. "Density Functional Theory Study on Stabilization of the Al_{13} Superatom by Poly(vinylpyrrolidone)", Tomomi Watanabe, Kiichirou Koyasu, and Tatsuya Tsukuda, *J. Phys. Chem. C*, DOI: 10.1021/jp5107718

Oral presentations

1. "超原子 Al_{13} と PVP の相互作用：安定性と反応性に対する電子移動の効果", 渡辺智美, 小安喜一郎, 佃達哉, 第 8 回分子科学討論会, 広島, 2014 年 9 月.

Poster presentations

1. "New magic clusters of aluminum oxide, $Al_{14}O^-$ and $Al_{15}O_2^-$", Tomomi Watanabe, Hironori Tsunoyama and Tatsuya Tsukuda, International Symposium on Small Particles and Inorganic Clusters XVI, Leuven, Belgium, July 2012.
2. "新奇アルミニウム酸化物クラスター$Al_{14}O^-$, $Al_{15}O_2^-$の構造と反応性", 渡辺智美, 角山寛規, 山添誠司, 佃達哉, 第 6 回分子科学討論会, 東京, 2012 年 9 月. (優秀ポスター賞受賞)
3. "Structural Characterization of Unprecedented $Al_{14}O^-$ and $Al_{15}O_2^-$: Photoelectron Spectroscopy and Density Functional Calculations", Tomomi Watanabe and Tatsuya Tsukuda, Symposium on Size Selected Clusters, Davos, Switzerland, March 2013.
4. "PVP からの電子移動による超原子 Al_{13} の安定化", 渡辺智美, 小安喜一郎, 佃達哉, ナノ学会第 12 回大会, 京都, 2014 年 5 月.
5. "Electronic shell closure of Al_{13} by electron donation from PVP", Tomomi Watanabe, Kiichirou Koyasu and Tatsuya Tsukuda, 17th International Symposium on Small Particles and Inorganic Clusters, Fukuoka, Japan, September 2014.

Acknowledgements

First of all, I would like to indebted to Professor Tatsuya Tsukuda for all he has done for me. Without his support, none of this works have been possible. His educational guidance always encouraged me to promote myself.

I am really thankful to Associate Professor Kiichirou Koyasu for discussing and giving me many advice through whole this work. I would like to express my acknowledgement to Assistant Professor Seiji Yamazoe for important suggestions and technical supports.

I am grateful to Associate Professor Miho Yamauchi (Kyusyu Univ.) and Lecturer Hironori Tsunoyama (Keio Univ.) for professional discussion of initial stage of this work. I'm thankful to Assistant Professor Jun-ichi Nishigaki (Tokyo Metropolitan Univ.) for giving me useful suggestions about experiments. I also would like to express my appreciation to Professor Tetsuya Taketsugu (Hokkaido Univ.) for great advices about DFT calculation part.

I'd like to appreciate to Ms. Yuka Sakurai for support me mentally. I am grateful to group member, Mr. Satoru Muramatsu, Mr. Akimaro Yanagimachi, Mr. Ryohei Tomihara, Mr. Keisuke Hirata, Mr. Sojiro Emori, and Mr. Kazuyuki Tsuruoka for daily discussion and kindly support, as well as to Mr. Shinjiro Takano, Ms. Setsuka Arii, Mr. Masaru Urushizaki, Mr. Ryo Takahata, Mr. Shun Hayashi, Mr. Syota Matsuo, Mr. Ryo Ishida, Mr. Yuichiro Kawahara and Mr. Tatsuya Higaki.

Finally I deeply appreciate to my family and friends for their understanding and continuous support.

Tomomi Watanabe

February 2015